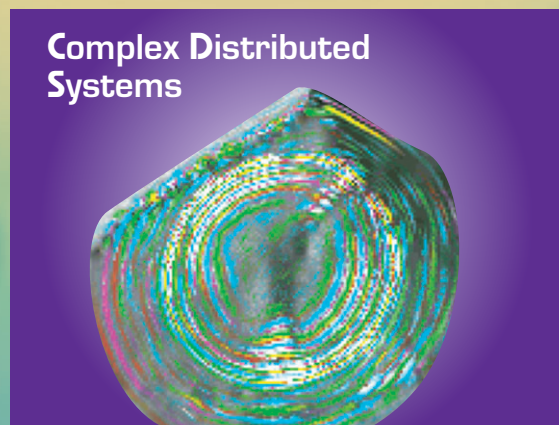
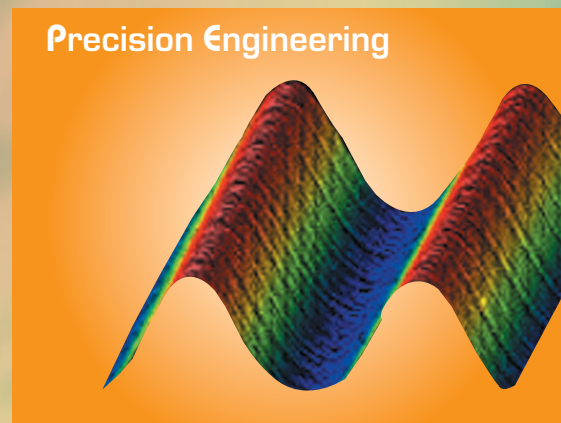
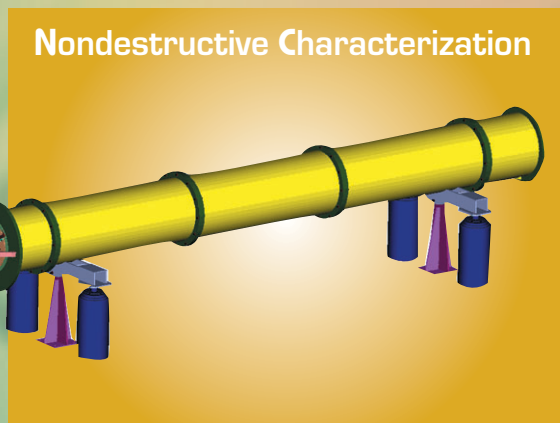
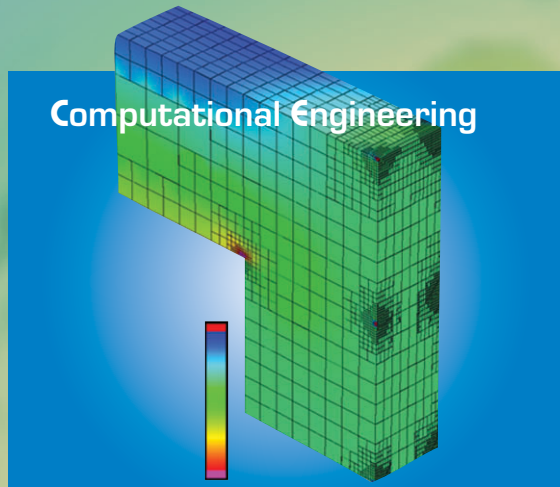
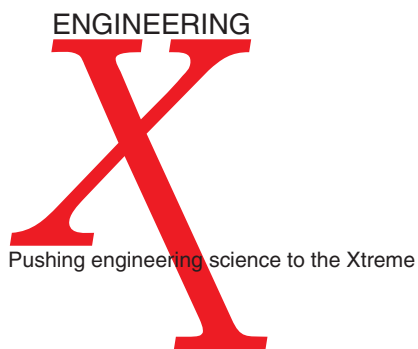


FY03

Engineering Technology Reports

Laboratory Directed Research and Development





Acknowledgments

Scientific Editing

Camille Minichino

Graphic Design

Irene J. Chan

Art Production/Layout

Jeffrey Bonivert

Debbie A. Marsh

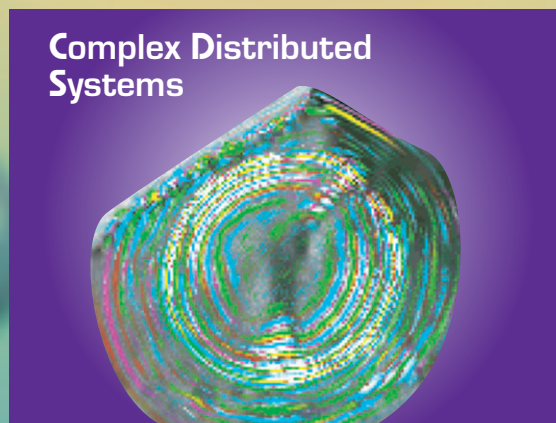
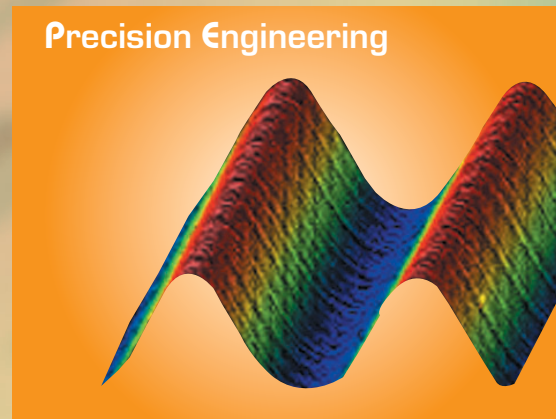
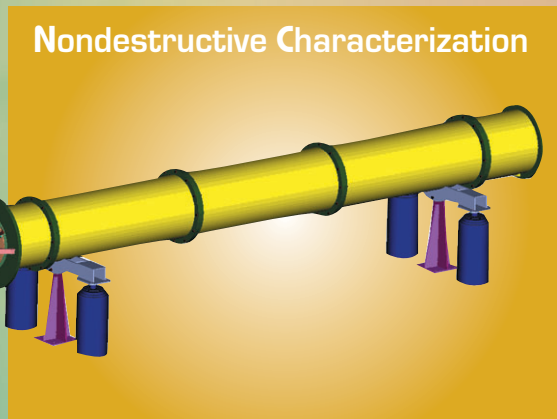
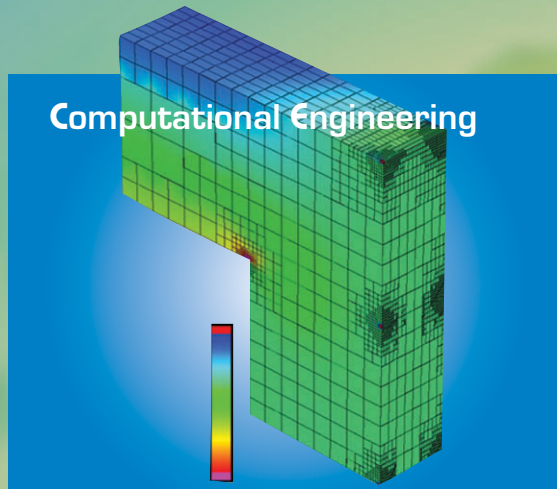
Kathy J. McCullough

Cover:

Graphics representing LDRD projects from
Engineering's Technology Centers.

FY03 Engineering Technology Reports

Laboratory Directed Research and Development



Introduction

Steven R. Patterson	.iii
---------------------	------

Center for Computational Engineering

Adaptive Mesh Refinement Algorithms for Parallel Unstructured Finite-Element Codes

D. Parsons, J. M. Solberg	.3
---------------------------	----

Analysis and Optimization of Novel Filtration, Sample-Collection and Sample-Preparation Systems

D. S. Clague, T. H. Weisgraber	.4
--------------------------------	----

Generalized Methods for Finite-Element Interfaces

M. A. Puso, J. M. Solberg	.5
---------------------------	----

Higher-Order, Mixed Finite-Element Methods for Time-Domain Electromagnetics

N. K. Madsen, D. A. White, N. J. Champagne	.6
--	----

Hypersonic Flow about Maneuvering Vehicles with Changing Shapes

F. F. Felker, V. M. Castillo	.7
------------------------------	----

Modeling and Characterization of Recompressed Damaged Materials

R. C. Becker	.8
--------------	----

Propagation Models for Predicting Communication System Performance in Adverse Environments

H.-Y. Pao	.9
-----------	----

Center for Microtechnology and Nanotechnology

Deterministic, Nanoscale Fabrication of Mesoscale Objects

R. P. Mariella, Jr., M. D. Shirk, G. H. Gilmer, A. M. Rubenchik, K. Carlisle	.13
--	-----

Disposable Polymerase Chain Reaction Device

E. K. Wheeler, W. J. Bennett, K. D. Ness, P. L. Stratton, A. A. Chen, A. T. Christian, J. B. Richards, T. H. Weisgraber	.14
---	-----

Integrated Microfluidic Fuel Processor for Miniature Power Sources

R. S. Upadhye, J. D. Morse, M. A. Havstad, D. A. Sopchak	.15
--	-----

Microfluidic System for Solution-Array-Based Bioassays

G. M. Dougherty, F. Y. S. Chuang, S. S. Pannu, K. A. Rose	.16
---	-----

Modeling Tools Development for the Analysis and Design of Photonic Integrated Circuits

T. C. Bond, J. S. Kallman, G. H. Khanaka	.17
--	-----

Reconfigurable Optical Code-Division Multiple Access for Fiber-Optic Networks

R. J. Welty, C. E. Reinhardt, N. P. Kobayashi, V. R. Sperry, I. Y. Han, E. M. Behymer, C. V. Bennett, S. W. Bond; Y. Du, S. J. Yoo (University of California at Davis)	.18
--	-----

Center for Nondestructive Characterization

Concealed Threat Detection at Multiple Frames/s

J. T. Chang, S. G. Azevedo, D. H. Chambers, P. C. Haugen, R. R. Leach, C. E. Romero, J. M. Zumstein; V. R. Algazi (University of California at Davis)	.21
---	-----

High-Accuracy X-Ray Imaging of Mesoscale Targets	
W. W. Nederbragt, T. W. Barbee, J. L. Klingmann, C. Vargas, H. E. Martz	22
Radial Reflection Diffraction Tomography	
S. K. Lehman, D. H. Chambers	23
Tabletop Mesoscale Nondestructive Characterization	
H. E. Martz, M. B. Aufderheide, T. W. Barbee, A. Barty, H. N. Chapman, J. A. Koch, B. J. Koziemiński, W. W. Nederbragt, D. J. Schneberk, G. F. Stone; M. Pivovarov (University of California at Berkeley)	24
Ultrasonic NDE of Multilayered Structures	
M. J. Quarry, K. A. Fisher; J. Rose (Pennsylvania State University)	25
Center for Precision Engineering	
High-Bandwidth Fast Tool Servo for Single-Point Turning High-Energy-Density Physics Targets	
R. C. Montesanti, J. L. Klingmann; D. L. Trumper (Massachusetts Institute of Technology)	29
Center for Complex Distributed Systems	
Cargo Container Security Sensor System	
S. G. Azevedo, K. E. Sale, B. D. Henderer, C. L. Hartmann-Siantar, J. Lehmann, L. S. Dauffy	33
Developing Smart Seismic Arrays	
P. E. Harben, D. B. Harris, S. C. Myers, S. C. Larsen, J. L. Wagoner, J. E. Trebes, K. E. Nelson	34
Evaluating a Regional Simulation Model for Seismic Wave Propagation	
H. Tkalcic, A. J. Rodgers, D. B. McCallen	35
Ultrawideband Communications	
F. U. Dowla, A. Spiridon, D. M. Benzel	36
Author Index	
	39

Introduction

Steven R. Patterson, Associate Director for Engineering

This report summarizes the science and technology research and development efforts in Lawrence Livermore National Laboratory's Engineering Directorate for FY2003, and exemplifies Engineering's 50-year history of researching and developing the engineering technologies needed to support the Laboratory's missions. Engineering has been a partner in every major program and project at the Laboratory throughout its existence, and has prepared for this role with a skilled workforce and the technical resources developed through venues like the Laboratory Directed Research and Development Program (LDRD). This accomplishment is well summarized by Engineering's mission: "Enable program success today and ensure the Laboratory's vitality tomorrow."

Engineering's investment in technologies is carried out through two programs, the LDRD program and the "Tech Base" program.

LDRD is the vehicle for creating those technologies and competencies that are cutting edge, or that require a significant level of research, or contain some unknown that needs to be fully understood. Tech Base is used to apply those technologies, or adapt them to a Laboratory need. The term commonly used for Tech Base projects is "reduction to practice."

Therefore, the LDRD report covered here has a strong research emphasis. Areas that are presented all fall into those needed to accomplish our mission.

For FY2003, Engineering's LDRD projects were focused on mesoscale target fabrication and characterization, development of engineering computational capability, material studies and modeling, remote sensing and communications, and microtechnology and nanotechnology for national security applications.

Engineering's five Centers, in partnership with the Division Leaders and Department Heads, are responsible for guiding the science and technology investments for the Directorate. The Centers represent technology areas that have been identified as critical for the present and future work of the Laboratory, and are chartered to develop their respective areas. Their LDRD projects are the key resources to attain this competency, and, as such, nearly all of Engineering's portfolio falls under one of the five Centers. The Centers and their Directors are:

Center for Computational Engineering:

Robert M. Sharpe

Center for Microtechnology and Nanotechnology:

Raymond P. Mariella, Jr.

Center for Nondestructive Characterization:

Harry E. Martz, Jr.

Center for Precision Engineering:

Keith Carlisle

Center for Complex Distributed Systems:

Donald Meeker (Acting Director)

FY2003 Center Highlights

The Center for Computational Engineering orchestrates the research, development, and deployment of software technologies to aid in many facets of the Laboratory's engineering mission. Computational engineering has become a ubiquitous component throughout the engineering discipline. Current activities range from tools to design the next generation of mixed-signal chips (systems on a chip) to full-scale analysis of key DOE and DoD systems.

Highlights of the Center's LDRD projects for this year include advances in finite-element methods, and modeling and simulation tools; hypersonic flow; modeling and characterization of recompressed damaged materials; and propagation models for communication system performance. The Center has offered a real-world computing capability that opens the door to solving a wide variety of fluid/solid interaction problems in transportation, aerospace, and infrastructure settings.

The mission of **the Center for Microtechnology and Nanotechnology** is to invent, develop, and apply microscale and nanoscale technologies to support the Laboratory missions in Stockpile Stewardship, Homeland Security, Nonproliferation, and other programs. The research topics for this Center cover materials, devices, instruments, and systems that require microfabricated components, including microelectromechanical systems (MEMS), electronics, photonics, micro- and nanostructures, and micro- and nanoactuators.

This year's projects include analysis and optimization of sample systems; integrated microfluidic fuel processor; microfluidic system for bioassay; modeling tools for photonic ICs; nanoscale fabrication of mesoscale objects; disposable PCR device; and optical code-division multiple access for fiber-optic networks.

The Center for Nondestructive Characterization (NDC) researches and develops nondestructive characterization measurement technology to significantly impact the manner in which the Laboratory inspects, and through this, designs, fabricates, and refurbishes systems and components. The Center plays a strategic and vital role in the research and development of scientific and engineering NDC technologies, such as acoustic, infrared, microwave, visible and x-ray imaging, to enable Engineering in the far- to mid-term to incorporate the successful technologies into Laboratory and DOE programs.

This year's LDRD projects include concealed threat detection at multiple frames/s; high-accuracy x-ray imaging of mesoscale targets; radial reflection diffraction tomography; tabletop mesoscale NDC; and ultrasonic NDE of multi-layered structures.

The Center for Precision Engineering advances the Laboratory's high-precision capabilities in manufacturing, dimensional metrology and assembly, to meet the future needs of the Laboratory and DOE programs. Precision engineering is a multi-disciplinary systems approach to achieve

an order of magnitude greater accuracy than currently achievable. Essential to the Center's success are its core technologies, which are the building blocks for the machines, systems, and processes that will be required for future programs. Our LDRD portfolio is driven to support this goal.

Highlights for this year include a high-bandwidth fast tool servo for single-point turning of high-energy-density physics targets, and our work with the other Centers on high-accuracy x-ray imaging of mesoscale targets and nanoscale fabrication of mesoscale objects.

The Center for Complex Distributed Systems (CDS) was formed to promote technologies essential to the analysis, design, monitoring and control of large-scale, complex systems. Given the ubiquitous nature of large systems, CDS obviously covers a very broad technical area. This includes development of integrated sensing, communication and signal processing systems for efficient gathering of the data essential for real-time system monitoring. The Center

also promotes the development of new methodologies for combining measured data with computer simulations in order to achieve enhanced characterization and control of complex systems.

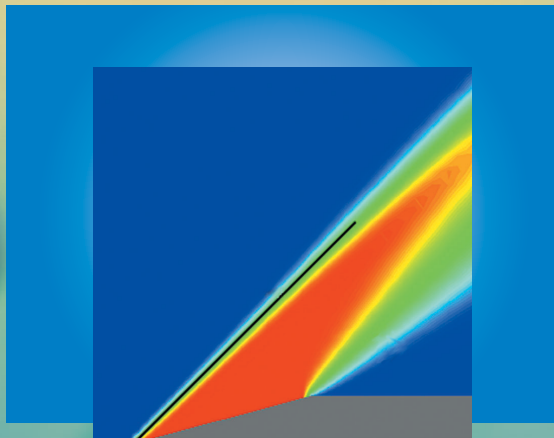
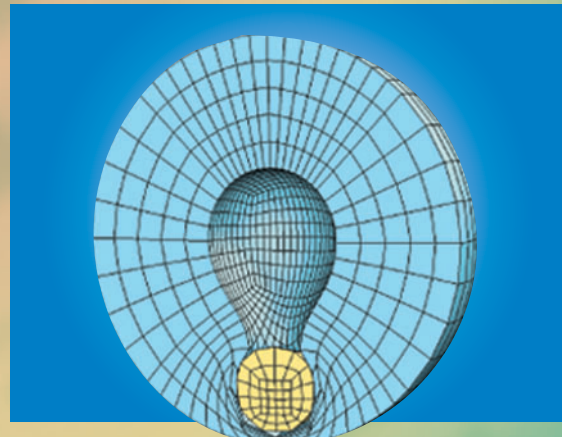
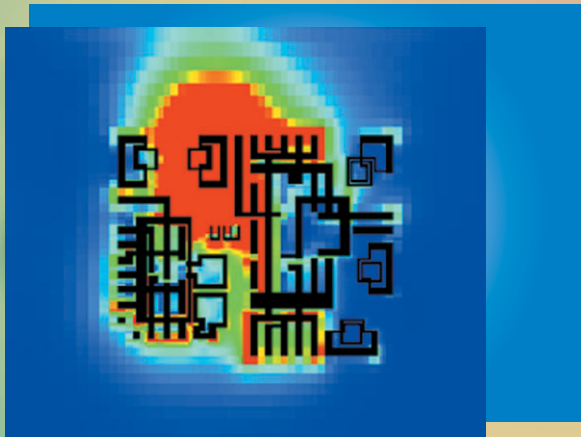
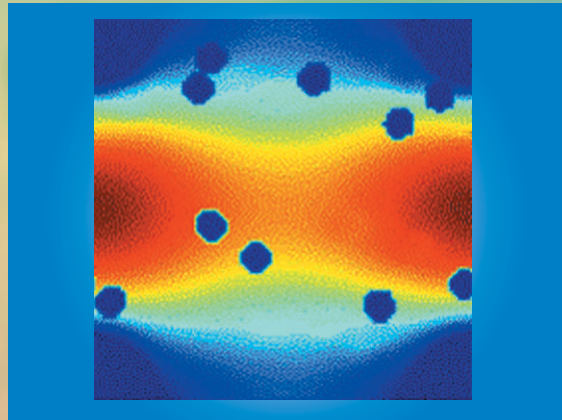
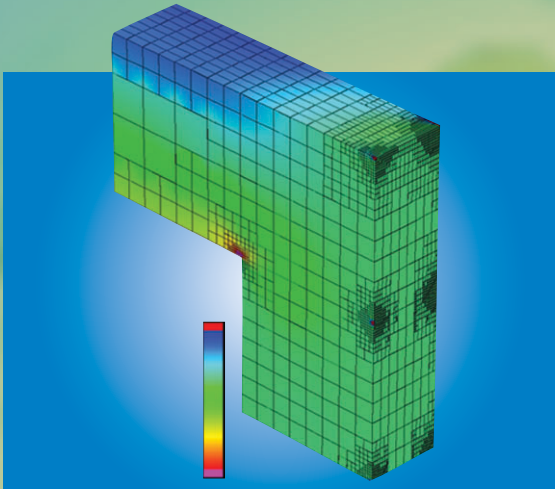
This year, the Center has LDRD projects in security sensor systems, seismic arrays and wave propagation, and communications. Particular emphasis is on technologies applicable to national security missions.

Science-Based Engineering

Our five Centers develop the key engineering technologies that make Laboratory programs successful. They provide the mechanism by which Engineering can help programs attract funding, while pioneering the technologies that will sustain long-term investment.

Our Centers, with staff who are full partners in Laboratory programs, integrate the best of mechanical and electronics engineering, creating a synergy that aids Engineering's mission, and helps turn the impossible into the doable.

Center for Computational Engineering



At LLNL, the state-of-the-art solvers used for solid mechanics simulations have sufficient architectural and functional maturity to benefit from the introduction of appropriate adaptive mesh refinement (AMR) strategies. These new tools will enable analysts to conduct more reliable simulations at reduced cost, in terms of both analyst and computer time.

Previous academic research in the field of AMR has produced voluminous literature focused on error estimators and demonstration problems. Relatively little progress has been made on producing efficient implementations suitable for large-scale problem solving on state-of-the-art computer systems. Research issues that we will consider include: effective error estimators for nonlinear structural mechanics problems, local meshing at irregular geometric boundaries, and constructing efficient software for parallel computing environments.

To date, progress has been made in three areas: construction of the serial software infrastructure, development of error estimators, and development of test problems.

Serial software infrastructure. Both isotropic and anisotropic h -refinements are permitted. Isotropic refinement is directionally invariant, causing a single hexahedron to be refined into eight new hexahedrons. Anisotropic refinement requires that the error estimator identify local element directions for refinement.

This may cause a hexahedral element to be split into two or four new elements. Anisotropic refinement is useful for problems that contain strong directional dependencies, or for meshes that possess poor aspect ratios.

The basic data object used in the mesh refinement

Adaptive Mesh Refinement Algorithms for Parallel Unstructured Finite-Element Codes

D. Parsons, J. M. Solberg

The objective of this research is to develop adaptive mesh refinement algorithms in unstructured finite-element codes used for solving nonlinear solid mechanics problems on ASCI-class, multi-processor parallel (MPP) computers.

procedures is the AMR block, which can be viewed as a single hexahedral element on the initial coarse mesh presented for adaptive refinement. Isotropic or anisotropic refinement is implemented as refinement of the individual AMR blocks, which in turn produces new elements and nodes in the AMR database that are eventually transferred to the global mesh database. During the refinement procedures, the elements and nodes in an AMR block are referenced using two sets of octrees. Manipulation of selected elements and nodes is then readily achieved using suitable recursive procedures.

Error estimators. Both patch-based recovery and residual-based error estimators are being developed. Patch-based recovery procedures smooth computed solution gradients to produce an improved estimate of the true solution; the estimated error is then the difference between the original and smoothed solutions. Residual-based procedures reflect the degree to which the computed solution satisfies the governing equations. Future work will explore

improvements to these basic methodologies that are pertinent to solid mechanics problems.

Test problems. Various test problems can be used to verify the AMR procedures described above. Figure 1 shows sequences of meshes generated using isotropic and anisotropic h -refinement of a single AMR block. The refinements

were performed using a random selection of elements and random refinement directions. Both sequences of meshes were used in a patch test to verify the computations. Figure 2 shows computed stress and temperature gradient fields in a symmetric portion of a square plate with a square hole subjected to both mechanical and thermal loads. Localized mesh refinement near stress singularities and thermal point fluxes is evident, demonstrating the viability of the AMR scheme for a coupled mechanics problem.

In FY04 the AMR functionality will be parallelized for efficient performance on MPP systems by introducing mesh-partitioning capabilities for allocating load-balanced subassemblies of a refined unstructured mesh to the available processors. The effectiveness of published algorithms for estimating discretization errors and for interpolating state variables to refined meshes will be investigated and improved.

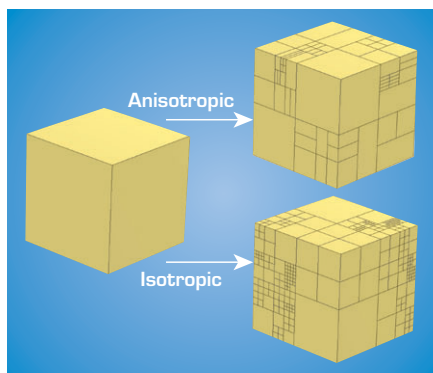


Figure 1. Meshes generated using isotropic and anisotropic h -refinement.

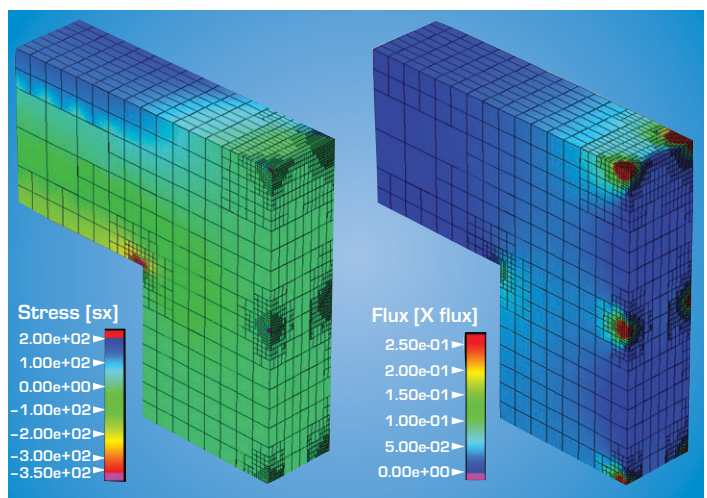


Figure 2. Stress and temperature gradient fields in a plate subjected to mechanical and thermal loads.

To accomplish our goals, we are developing new lattice-Boltzmann simulation tools that include detailed microstructure descriptions, relevant surface interactions, temperature effects, and the ability to handle both liquid and gas phase systems. The new capability is being validated with experimental data and will be applied to real-world issues of concern to LLNL programs.

This work directly impacts continuing and future LLNL efforts that involve filtration, collection and sample preparation. This capability will be directly applicable to detection systems relevant to LLNL's medical technology program, chemical and biological counter-proliferation mission, and homeland security mission.


Analysis and Optimization of Novel Filtration, Sample-Collection and Sample-Preparation Systems

D. S. Clague, T. H. Weisgraber

With the heightened attention on chemical and biological early-detection systems, there is an increased need for high-efficiency filtration, sample-collection and sample-preparation systems. The goal of this research project is to provide new computational analysis tools designed to optimize these critical operations and to characterize system efficiencies based on the details of the microstructure with environmental effects.

This project was a late mid-year start in FY02. In FY03, we achieved four major milestones: 1) development of the media module, which includes various arrangements of cylindrical obstacles and porous membranes with a controllable distribution of pore sizes (Fig. 1); 2) development of the capability

to characterize hindered transport coefficients in complex media (Fig. 2); 3) inclusion of particle-particle and particle-medium colloidal interactions, e.g., van der Waals and electrostatics; and 4) incorporation of an energy equation to handle thermal effects.

The proposed new developments for FY 04 include the completion of fluid species transport studies in membranes and the validation of predictions with data from the dialysis project. We are also working on including more complex geometries, e.g., cylinders, in support of the nano-bar code project. Finally, we will develop the ability to handle gas phase transport and gas phase with particles in porous media with surface forces. 

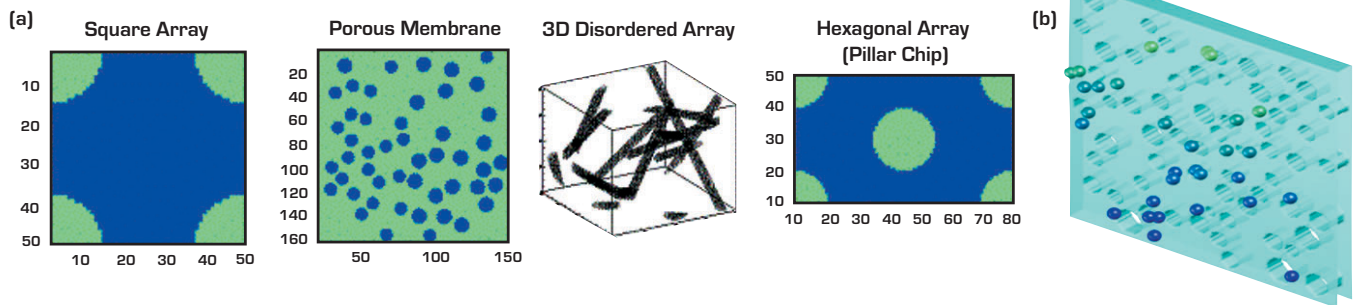


Figure 1. (a) Media generated on demand. Three arrangements of cylinders, including the pillar chip, and a porous membrane with specified porosity and pore size distribution. (b) 3-D perspective of porous membrane with mobile species.

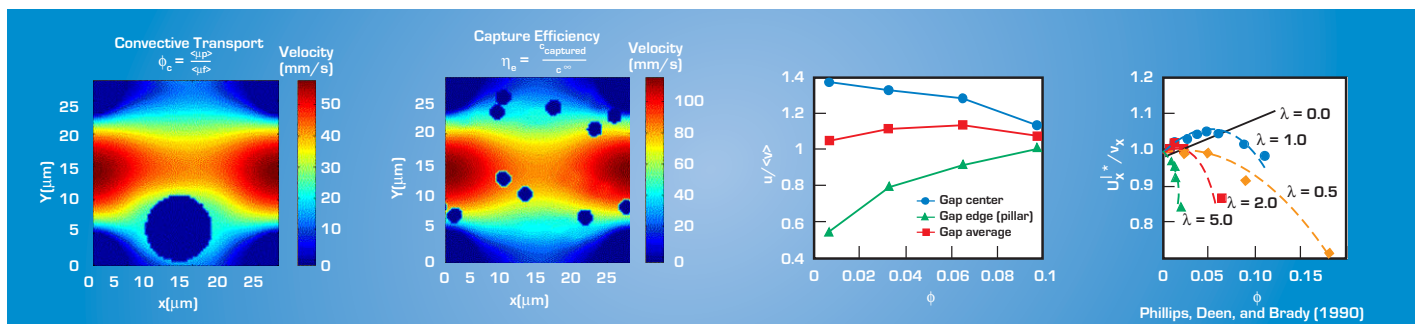


Figure 2. Results from characterization of hindered convection and species capture in a regular array of cylinders. The hindered transport coefficient as a function of volume fraction and position within the gap between cylinders is shown.

Mesh generation is now the main bottleneck in computer-aided analysis. Much of the effort in the production of a complex finite-element model is the interfacing of individual parts at part boundaries. When individually meshed parts are to be connected to form a single monolithic part, analysts work very hard to ensure that the meshes conform at the part interfaces, *i.e.*, that the nodes match at the common boundary.

The process of producing conforming meshes is one of the main difficulties in mesh generation and is intractable and sometimes impossible when connecting meshes composed of different element types [see Fig. 1]. Although standard mesh tying methods are an alternative to producing conforming meshes, it is well known that they cause large errors and are avoided. Consequently, a method that can connect (tie) dissimilar meshes accurately would be an effective tool in mesh production and significantly simplify analyst efforts. Furthermore, dissimilar (non-conforming) meshes are unavoidable when parts are interfaced via contact surfaces [see Fig. 2]. Despite their common use, contact surfaces still cause serious analysis problems, such as inaccuracies and code crashing.

The goal of this project is to research and develop *robust* and *accurate* methods for interfacing (*i.e.*, tying and contacting) dissimilar meshes. This new technology could save a significant amount of time and money invested in mesh production. For example, a large weapons model takes a month to build and will undergo many revisions over a matter of years. Analysts estimate that an accurate method for tying dissimilar meshes could save 10 to 25% of their time in meshing over the course of a project.

Furthermore, analysts spend a significant amount of time dealing with problems related to contact surfaces, particularly for *implicit* finite-element analysis. The new, more robust approach should make analysis with contact surfaces more accurate and more reliable.

The “mortar method” for connecting 2-D, flat interfaces has been extended to

Generalized Methods for Finite-Element Interfaces

M. A. Puso, J. M. Solberg

The goal of this project is to research and develop robust and accurate methods for interfacing dissimilar meshes. In FY03, we worked on a mortar implementation that can connect meshes with different element types.

connect arbitrary 3-D, curved meshes so that optimal convergence is achieved. In this way, refinement of the dissimilar mesh will have the same asymptotic convergence rate as the conforming mesh, thus dissimilar meshing will not compromise accuracy. This method requires solving surface integrals involving Lagrange multiplier fields for traction and displacement. Such surface integrals are straightforward for 2-D, flat interfaces but complicated for 3-D, curved surfaces.

In FY01, we developed a closest-point projection type algorithm for 3-D surface integrals and used simple Lagrange multiplier fields to demonstrate optimal convergence on 3-D models with curved, tied interfaces.

connect arbitrary 3-D, curved meshes

so that optimal convergence is achieved. In this way, refinement of the dissimilar mesh will have the same asymptotic convergence rate as the conforming mesh, thus dissimilar meshing will not compromise accuracy. This method requires solving surface integrals involving Lagrange multiplier fields for traction and displacement. Such surface integrals are straightforward for 2-D, flat interfaces but complicated for 3-D, curved surfaces.

In FY02, we further developed our theory for stability conditions; implemented a dual formulation for the Lagrange multiplier fields, which sped calculation times by a factor of seven over our previous results; and began work on the mortar method for contact. In FY03, we worked on a mortar implementation that can connect meshes with different element types (*i.e.*, tetrahedrals and quadratic elements). Now, automatically generated tetrahedral meshes can be accurately interfaced with hexahedral meshes [Fig. 1.] Friction was also added to the mortar contact. The new mortar contact provides vastly superior non-linear convergence behavior since it effectively smoothes the behavior near the interface and eliminates the “locking” associated with the standard contact methods. Consequently, contact analyses that failed [crashed] in the past can be successfully analyzed using *implicit* finite elements with our new mortar approach [Fig. 2].

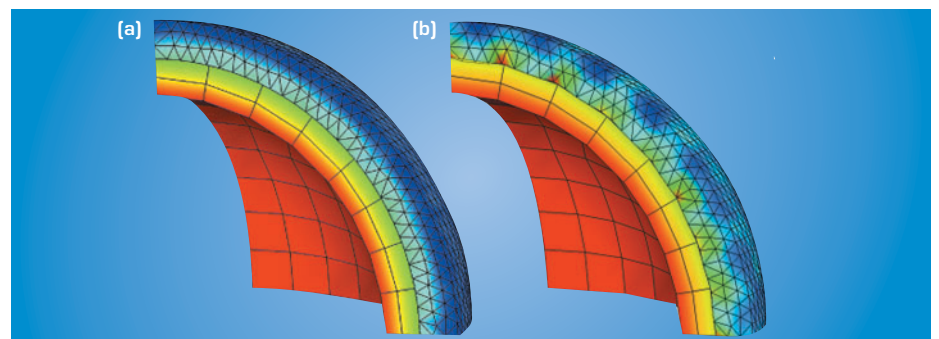


Figure 1. Tied hexahedral-tetrahedral mesh of internally pressurized sphere. (a) Mortar tying produces smooth stresses with stress error at boundary of 1.78%. (b) The standard tying method yields non-smooth stresses with stress error of 220% at boundary.

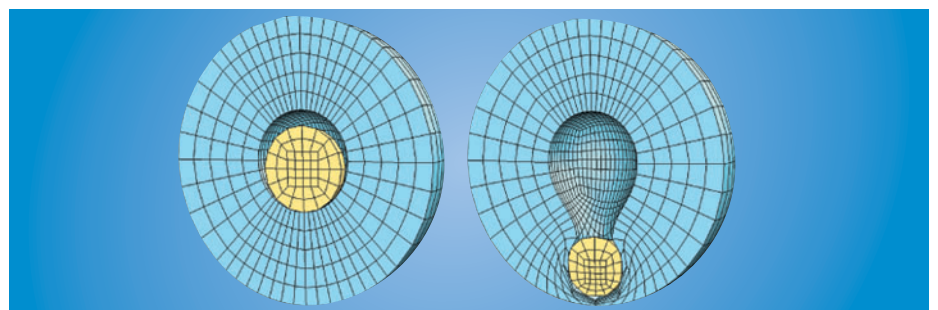


Figure 2. Elastic sphere forced into thick elastic shell. Analysis performed with implicit finite-element method using mortar contact. Standard contact methods cannot nearly approach this significant amount of deformation with implicit finite elements.

Time-domain computational electromagnetic (CEM) modeling is the most cost-effective approach for EM design and analysis for problems that are electromagnetically very large or are nonlinear and transient in nature. However, no stable, higher-order, conservative methods, such as those that exist for computational fluid dynamics and other disciplines, exist for time-domain CEM, largely because of the unique characteristics possessed by Maxwell's equations.

Typically Maxwell's equations are solved with low-order, Cartesian-grid methods. These simple, stable methods work well for rectangular geometries but require prohibitively large meshes for quantitative field predictions on electrically large problems, and produce inconsistent solutions for non-orthogonal geometries. In addition, finite-volume schemes, which are often considered as an alternative, suffer from numerical instabilities, lack of conservation, and low accuracy.

To overcome these limitations, this project investigated higher-order, mixed finite-element methods (MFEM), a new methodology for solving partial differential equations on 3-D unstructured grids. Our goal is to develop a stable, conservative, higher-order accurate simulation code for Maxwell's equations and related EM equations. Our MFEM methodology builds on LLNL's competency in computational engineering and will 1) enable engineers to perform EM simulations on unstructured grids, and 2) provide a coupled electro-thermal-mechanical modeling capability, both in support of the Laboratory's national security mission.

Accomplishments in FY03 include 1) completing the core higher-order numerical components of our simulation code, such as integration rules, basis functions, and the hexahedron, tetrahedron, and prism elements; 2) developing higher-order non-dissipative time-integration methods; and 3) completing a prototype massively parallel MFEM code for Maxwell's equations.

Higher-Order Mixed Finite-Element Methods For Time-Domain Electromagnetics

N. K. Madsen, D. A. White, N. J. Champagne

This project is investigating higher-order, mixed finite-element methods — a new methodology for solving partial differential equations on 3-D unstructured grids. Our goal is to develop a stable, conservative, higher-order accurate simulation capability for Maxwell's equations and related equations of electromagnetism.

To demonstrate the accuracy and efficiency of our approach we compute the resonant frequencies of a sphere using higher-order "curved" basis functions for spatial discretization and a higher-order symplectic integration for temporal discretization. The results are shown in Fig. 1. For the same accuracy, the higher-order code (3rd order in space and time) required 896 times fewer elements and ran 43 times faster.

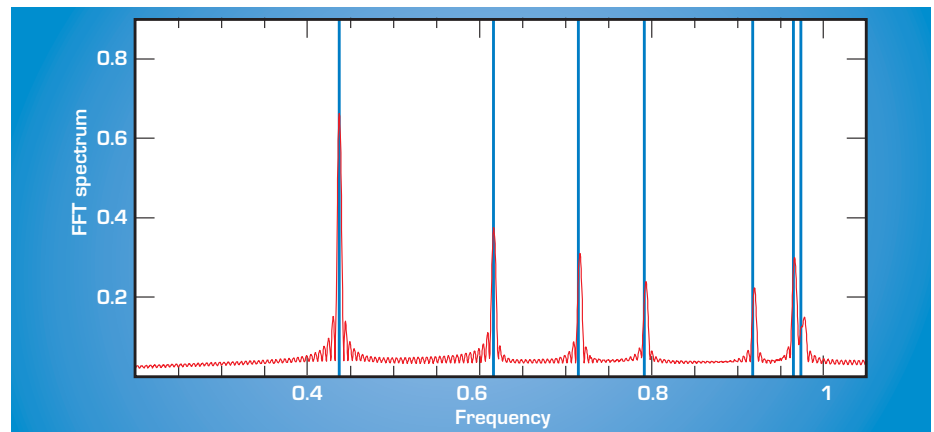


Figure 1. Computed resonant frequencies (red) compared to exact solution (blue). The new higher-order algorithm is 43 times more efficient for this problem than standard-order algorithms.

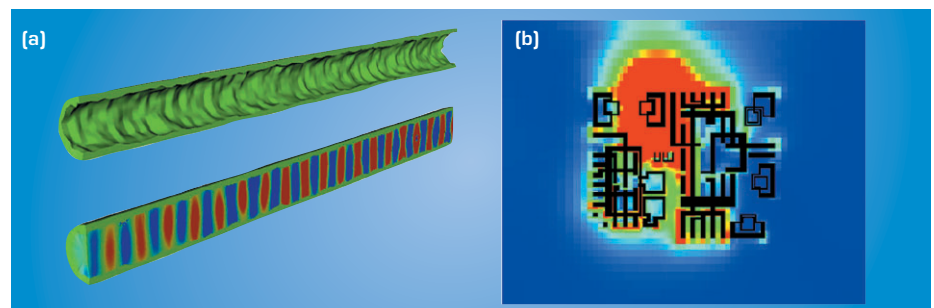


Figure 2. (a) Electromagnetic wave propagation in a rough-surface tunnel. (b) Electric fields in an integrated circuit substrate.

In Fig. 2 we illustrate two applications that require high-fidelity EM simulations. Figure 2 (a) shows an EM wave propagating in a random rough-surface tunnel. The goal of this simulation is to characterize the dispersion and attenuation of the wave for communication system performance. Figure 2 (b) shows the electric field intensity in a high-frequency analog integrated circuit.

The goal of this simulation is to gain insight in substrate coupling effects that are becoming increasingly important in circuit design.

Possible future research activities in this area include adaptive mesh refinement, improved absorbing boundary conditions, and coupled electro-thermal-mechanics simulations.



Vehicles moving at hypersonic speeds have great importance to LLNL's national security mission. Ballistic missile re-entry vehicles (RVs) travel at hypersonic speeds, as do missile defense intercept vehicles. Despite the importance of the problem, no computational analysis method is available to predict the aerodynamic environment of maneuvering hypersonic vehicles, and no analysis is available to predict the transient effects of their shape changes. The present state of the art for hypersonic flow calculations typically still considers steady flow about fixed shapes. Additionally, with present computational methods, it is not possible to compute the entire transient structural and thermal load for RVs.

The objective of this research is to provide the required theoretical development and computational analysis tool. This key enabling technology will allow the development of a complete multi-mechanics simulation of the entire RV flight sequence, including important transient effects such as complex flight dynamics. This will allow the computation of the as-delivered state of the payload in both normal and unusual operational environments. This new analysis capability could also provide the ability to predict the nonlinear, transient behavior of end-atmospheric missile interceptor vehicles to the input of advanced control systems.

Due to the computational intensity of fluid dynamics for hypersonics, the usual approach for calculating the flow about a vehicle that is changing shape is to complete a series of steady calculations, each with a fixed shape. However, this quasi-steady approach is not adequate to resolve the frequencies characteristic of a vehicle's structural dynamics.

Our approach is to include the effects of the unsteady body shape changes in the finite-volume method by allowing for arbitrary translation and deformation of the control volumes. Furthermore, because the Eulerian computational

Hypersonic Flow about Maneuvering Vehicles with Changing Shapes

F. F. Felker, V. M. Castillo

The objective of this research is to provide the required theoretical development and a computational analysis tool for calculating the hypersonic flow about maneuvering, deforming re-entry vehicles.

mesh for the fluid domain must be attached to the vehicle as it undergoes potentially high accelerations, that mesh must be viewed in a non-inertial coordinate frame. The usual conservation-law form of the fluid dynamic governing equations must be augmented. This approach thus requires the derivation of a significant new numerical formulation, especially to incorporate a modern flux-splitting methodology as needed for numerical stability and accuracy.

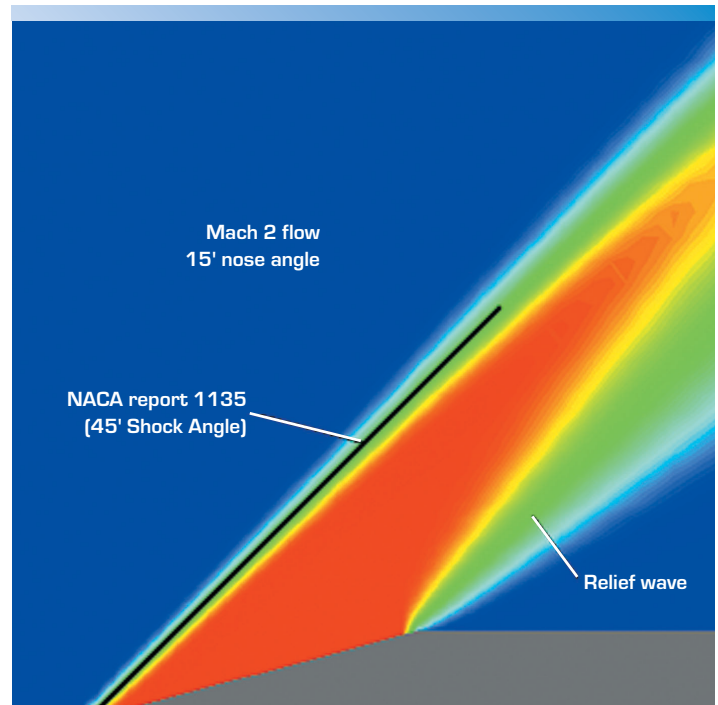
In FY03 much of the numerical formulation was conceptualized, derived, and documented. This initial effort concentrated on the deforming, non-inertial mesh considerations in the context of inviscid flows. We are making contacts in the academic community, seeking an independent review of this work, and anticipate a future publication. With that baseline established, the numerical formulation must be augmented to consider effects of viscosity and other "diffusive" mechanisms. Reactive chemistry is another component that must be added to achieve our

eventual goals for hypersonic flow simulation.

The implementation of this new methodology is being supported through LLNL programs. A "born parallel" computer code, RVFlow, is being written within the Diablo framework. The code takes advantage of some of the sophisticated features of

Fortran90 to pass data structures in an efficient manner. A steady inviscid capability with explicit time integration has been prototyped.

To demonstrate the accuracy of the code, we use a series of verification tests including simulations of a shock tube and simulations of various shapes in a hypersonic flow field (see figure). The shock tube simulation results show extremely sharp shock wave profiles. These demonstrate the advantage of using the flux-splitting method. Test cases simulating a wedge shape in various flow fields up to Mach 20 show good agreement with known results for the shock angles.



Calculated pressure of a low-Mach-number flow, showing the predicted shock angle and relief wave.

The severity of the damage from spall ranges from isolated voids to full fracture of the material by void coalescence. In many situations the material is subjected to secondary loading which acts to close the spall-related voids. While much work has been done to characterize and model spall damage, little has been done to understand and model the recompression process.

Prior experimental work under this project involved creating spall-damaged samples in a gas gun, performing recompression in a dynamic split-Hopkinson bar apparatus, and evaluating the strength of the resulting specimen. The results showed that the voids were not closed under the conditions obtained in the Hopkinson bar, even though the voids occupied a significant fraction of the cross-section at the spall plane.

Further numerical analysis showed that strain hardening of the copper near the voids was responsible for the nonclosure. The strength locally around the voids was significantly higher than the original strength of the material so, when compressed, deformation occurred outside of the voided region. These results indicated that stress states with higher triaxiality are required to close the porosity. This led to additional experiments and simulations under conditions that would produce higher pressures.

In the current phase, experiments were run on lasers and gas guns to impose the recompression. For the laser experiments, spall damage was induced on thin samples by direct ablation of the copper target. This produced spall and, in most cases, a visible blister on the backside of the specimen. The samples were recovered and coated on the backside with an ablative layer. These were then reshocked with the

Modeling and Characterization of Recompressed Damaged Materials

R. C. Becker

Materials subjected to dynamic loading from high-velocity impacts or explosives frequently incur internal damage in the form of spall. Spall in metals is characterized by nucleation and growth of voids under tensile loading conditions, created by the interaction of stress waves with surfaces and interfaces. The purpose of this work is to examine the recompression of spall-damaged materials experimentally and to develop a model capturing the recompression response.

laser focused on the prior spall blister to close the spall.

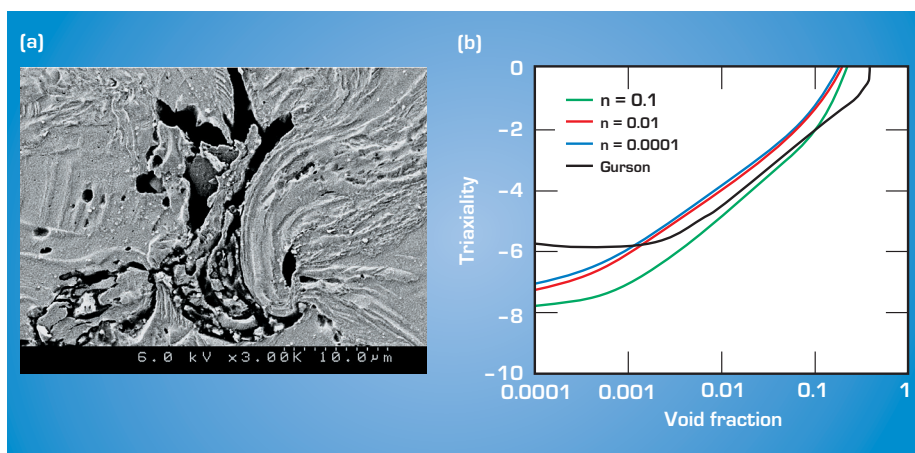
A micrograph from the recompressed spall region is presented in the figure (a). This shows a void partially collapsed by a jetting mechanism entering from the right. There appears to be a particle in the collapsed cavity. This may be the particle responsible for initiating the void in the initial spall process. On a larger scale, it appears that the once-separated spall plane has been closed, but significant porosity remains.

Simulations of void growth and recompression in a periodic array were conducted to investigate how existing continuum level void models could be

adapted to reproduce the material response predicted by micromechanical simulations. Since strain hardening plays an important role in void closure, unit cell simulations were conducted using a range of strain hardening. The material response during recompression, represented in terms of stress triaxiality (hydrostatic stress divided by von Mises effective stress), is plotted against void fraction in the figure (b). Characterizing the behavior in terms of the

triaxiality provides a scaling relation that collapses the widely disparate response to a set of closely spaced curves.

Material point simulations using the Gurson void growth model were run under similar loading conditions. Model parameters were adjusted to obtain a reasonable fit to the triaxiality over a range of void fractions down to a fraction of a percent (see figure (b)). Based on these results, a viable model for recompression in large-scale continuum simulations can be obtained by using the Gurson model with different parameters than those used for formation of spall.



(a) Micrograph showing jetting of material accompanying void closure. (b) Triaxiality results for unit cell models with varying hardening and the Gurson model.

In addressing propagation models for communications in adverse environments, our goals are to investigate the propagation physics, develop the mathematical models, derive the statistical descriptors, specialize to radio communication in tunnels and caves, and select the models/methods best suited to the parameter space describing enclosures of interest.

In addition to the ongoing development of a bibliography of the relevant literature, analytical work during FY03 has focused on specific problems. These are 1) propagation of waveguide modes in a rough-walled quasi-circular perfect electrical conductor (PEC) waveguide; 2) calculation of the fields due to a horizontal electric dipole in a rectangular tunnel with two smooth PECs, and two smooth, lossy walls; 3) propagation of waveguide modes in a rough-walled tunnel, using an equivalent surface impedance to model the wall roughness; and 4) calculation of the fields produced in a circular smooth-walled tunnel by circularly symmetric electric and magnetic current loops.

Smooth-walled straight tunnels. The principal results of the analytical work on smooth-walled straight tunnels are the following:

Propagation Models for Predicting Communication System Performance in Adverse Environments

H.-Y. Pao

This project addresses the problem of characterizing the propagation of electromagnetic fields in the adverse environments that are encountered in enclosures such as caves, tunnels and urban canyons, where rough or complex bounding surfaces can compromise the quality of signals.

1. Sources should be polarized such that quasi-TE fields are preferentially excited, to reduce field attenuation. For a circular tunnel, this indicates a circular electric-current loop or a helix antenna.

2. Propagated field amplitudes can vary axially by 20 to 30 dB over short distances. Our results in this regard are consistent with theoretical and experimental results obtained in the past by other investigators.

3. Destructive interference among the modes or rays, in terms of which the field is represented, plays a critical role in determining the axial field attenuation.

Rough-walled waveguides. The principal results of the work on modal propagation in rough-walled waveguides are the following:

1. The total modal field can be decomposed into the sum of a deterministic or

coherent part and a zero-mean random or incoherent part. The coherent part of a given modal field has a structure similar to that of the field in a smooth-walled waveguide; the incoherent part tends to be concentrated near the waveguide wall.

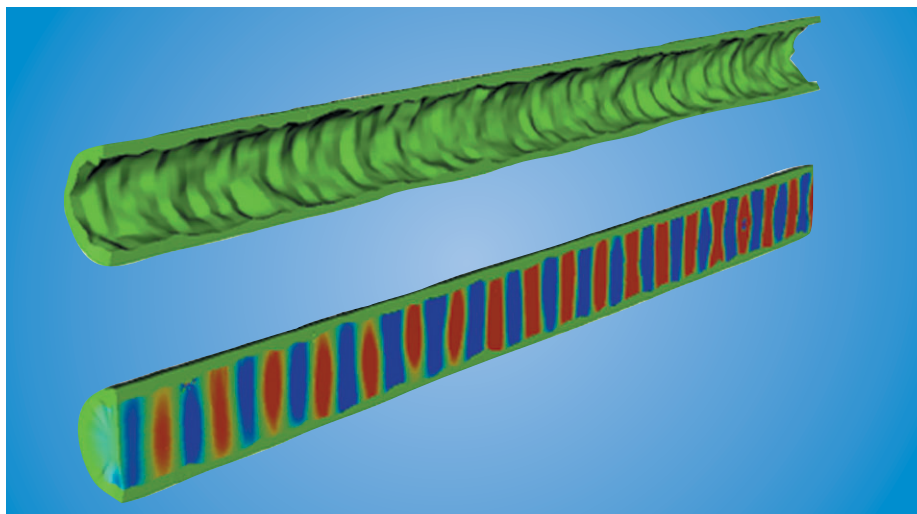
2. The modal cutoff frequencies are only slightly affected by the wall roughness; however, there is evidence that

certain of the waveguide modes can become slow (that is, the axial phase velocity of the mode can become less than the speed of light) above certain critical frequencies.

3. The auto- and cross-covariance functions that describe the incoherent part of the field can be expressed in terms of the power spectral density of the surface roughness.

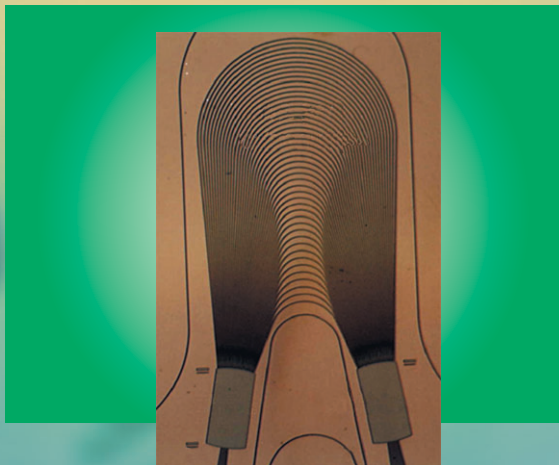
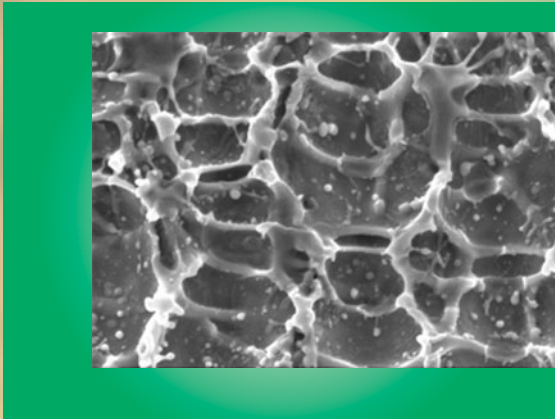
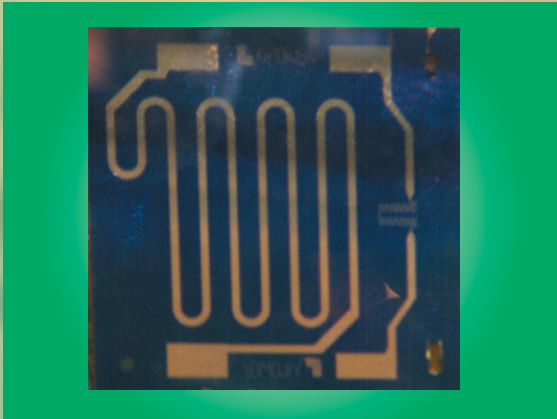
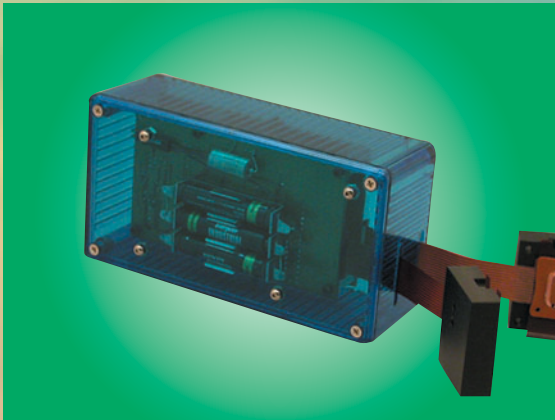
The work has led to papers presented at the North American Radio Science Meeting and at the International Conference on Electromagnetics in Advanced Applications.

In FY04 we will continue theoretical work, start analytic work on urban canyons, and perform experimental confirmation.



Electromagnetic wave propagation in a rough-surface tunnel.

Center for Microtechnology and Nanotechnology



We have chosen to use sub-ps laser pulses for our experiments because using lasers with pulses shorter than the electron-phonon relaxation time (under 1 ps) offers the most precise control of the energy that can be deposited into a metal surface. From the standpoint of scientific understanding, pure, elemental metal targets, including single-crystal targets, were optimal.

The use of sub-ps laser pulses also allowed a decoupling of the energy-deposition process from the ensuing movement/ablation of the atoms from the solid, which simplified the modeling. We have compared ablation of material from copper and gold, which behave similarly [due to their high thermal conductivity] with nickel substrates (Fig. 1).

In FY03, we combined the power of the 1-D hydrocode HYADES with state-of-the-art, 3-D molecular-dynamics (MD) simulations. The studies of material ablation by the short laser pulses consider the scales of materials modification and ejecta that are much smaller than the laser spot; thus a 1-D treatment of the problem is adequate. The code takes into account the change of the absorption during the pulse due to the change of electron density, spatial profile, and temperature.

Deterministic, Nanoscale Fabrication of Mesoscale Objects

R. P. Mariella, Jr., M. D. Shirk, G. H. Gilmer,
A. M. Rubenchik, K. Carlisle

No organization has the capability to perform deterministic fabrication of mm-sized objects with arbitrary, μm -sized, 3-D features with 20-nm-scale accuracy and smoothness. For deterministic fabrication of high-energy-density physics targets, it will be necessary both to fabricate features in a wide variety of materials and to understand and simulate the fabrication process. We continue to investigate, both in experiment and in modeling, the ablation/surface modification processes that occur with the use of fs laser pulses that are near the ablation-threshold fluence.

The equation of state quantities and related thermodynamics coefficients were obtained from external tables. For the interaction with metals we used the Thomas-Fermi model. Material electromagnetic properties are described with an extended Drude model that includes both intraband and interband transitions.

Laser ablation was modeled using large-scale MD simulations [via the parallel code MDCASK] (Fig. 2) of single-crystal copper. The computational cells contained from four to thirty million atoms. Interactions between the copper atoms were simulated using the embedded atom potential.

The description of thermal transport includes temperature-dependent thermal conduction and heat capacities. Thermal conduction is determined by the collision frequency in the Drude model. The cold value of transport constants are matched with experimental

data and interpolated to the hot plasma expression for an ideal plasma.

A rich diversity of phenomena was observed as a function of the pulse energy density, including the ejection of a liquid film. Three distinct regimes are exhibited: 1) a low-energy regime with a minute ablation flux corresponding to evaporation of atoms from the hot copper surface; 2) an intermediate regime

where void nucleation and growth, or spall, causes the ejection of a stable liquid layer and particles; and 3) high-pulse energies where liquid droplets are ejected with a wide range of sizes.

Published observations of interference fringes during fs ablation are in excellent agreement with our simulations that show the ejection of a liquid layer.

One important finding is that the ablation process inevitably generates subsurface voids that ultimately can freeze out as undesirable residual surface roughness. Another important discovery is that initial surface scratches tend to nucleate the instabilities that ensue during laser ablation. Post-ablation surface processing may be able to reduce these residual surface features to sub-20-nm sizes.

We have documented our progress with conference presentations and publications, as well as a record of invention (IL-11139).

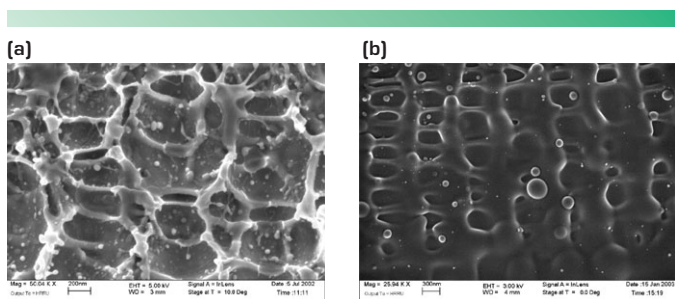


Figure 1. Micrograph surfaces of (a) copper and (b) nickel, after ablation with 150-fs laser pulses, showing the relatively smoother surface of the nickel.

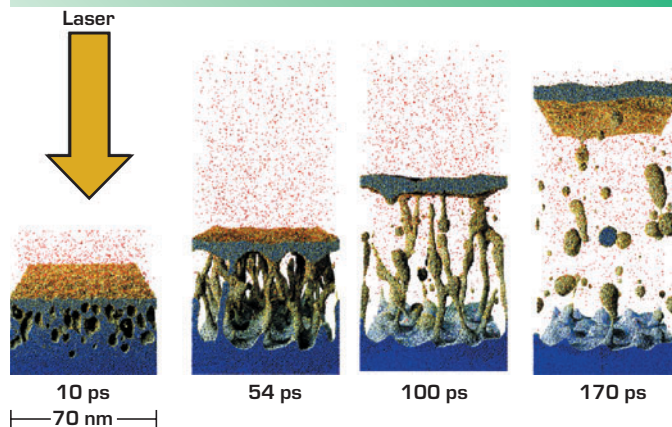


Figure 2. Graphical output of molecular-dynamics simulations of laser ablation, showing subsurface nucleation, growth, and coalescence of nm-scale voids that lead to spall.

To take appropriate action, first responders to a biological attack (local emergency response personnel, military, or intelligence personnel) must identify the specific organism released. For this purpose, polymerase chain reaction (PCR) assays are becoming increasingly important because they can amplify a target segment of DNA (by thermal cycling of the necessary reagents) and enable identification of pathogens.

We have designed and demonstrated a compact, disposable PCR thermal cycler. The convectively-driven PCR (CPCR) thermal cycler uses thermal convective forces created by fixed, nonfluctuating, hotter- and cooler-temperature regions to thermally cycle the sample fluid to achieve amplification. Buoyancy forces cause the fluid to flow through the different temperature zones.

The advantage of this approach is lower power requirements, ensuring that small batteries will suffice as the system's power source. The thermal cycler is also fabricated from inexpensive material, making it affordable to more customers.

Disposable Polymerase Chain Reaction Device

E. K. Wheeler, W. J. Bennett, K. D. Ness, P. L. Stratton, A. A. Chen, A. T. Christian, J. B. Richards, T. H. Weisgraber

The September 11, 2001 attack on the United States and the subsequent anthrax scare have raised antiterrorist vigilance to new heights. Although 9/11 was orchestrated with hijacked planes, the next threat could be nuclear, chemical, or—as evidenced by the anthrax scare—biological. Planning and equipping for a biological attack requires detection devices that are robust in the field, easy to use, and relatively inexpensive. This project has leveraged LLNL's competencies in microtechnology and instrumentation and provided new capabilities in support of LLNL's homeland security mission.

During FY03 we focused on testing and optimizing our novel CPCR thermal cycler on a biological surrogate, starting with genomic DNA. *Erwinia herbicola* (Eh) was chosen for its relevance to both medical and bio-warfare arenas. Both 58- and 160-bp segments of Eh were amplified in the CPCR thermal cycler. Agarose gel detection of an amplification of the 160-bp amplicon is shown in Fig. 1.

The central energy consumption requirement is to heat an aqueous fluid from room temperature to 95 °C and then to cycle the fluid between 55 °C and 95 °C. The CPCR device minimizes losses to the environment and maximizes the energy transferred to the

fluid. The energy consumed by the thermal cycler for 30 min of amplification for a 75-ml sample is 866 ± 50 J. The basic heat requirement for 50 cycles is 8.4 J/ μ l/run. For a typical 25- μ l sample size the basic energy requirement is 210 J/run. Compared to existing field deployable technologies, the CPCR thermal chamber lowers energy consumption per unit volume an order of magnitude.

Based on the low energy requirements of the device, we have fabricated a battery-operated thermal cycler, shown in Fig. 2. With our increased understanding, we have further optimized our selection of material properties and heater configurations.

We anticipate that this new and more energy efficient PCR device will not only see widespread use in the field, but could ultimately become pervasive in diagnostics such as food quality control, medical diagnostics, and environmental monitoring, and could also become a low-cost diagnostic for third world countries.

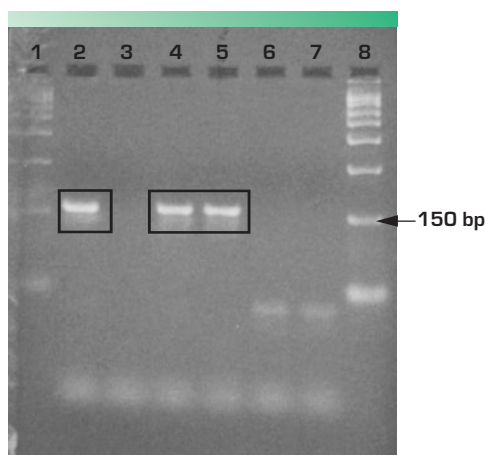


Figure 1. Gel detection showing successful amplification of a 160-base-pair (bp) segment of genomic *Erwinia herbicola* DNA, compared to amplification in a standard bench-top thermal cycler. Lanes 1 and 8 contain DNA markers (50-, 150-, 300-bp). Wells 2 and 3 are positive and negative controls, respectively, performed on a bench-top thermal cycler. Wells 4 and 5 are two aliquots from a CPCR run; wells 6 and 7 are negative controls from a CPCR run.

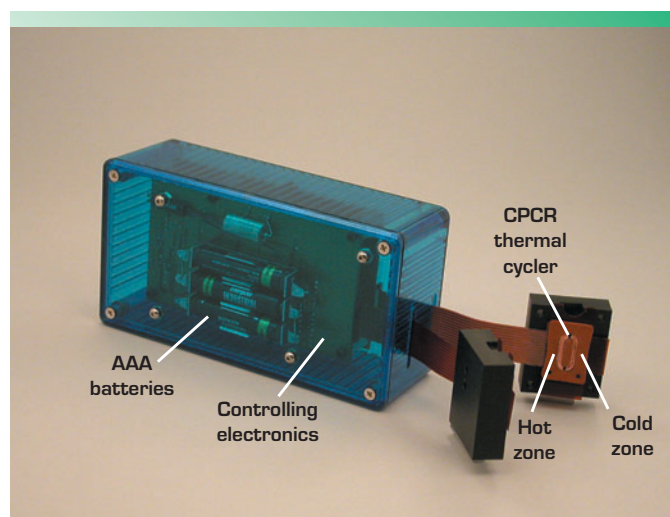
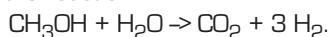


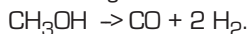
Figure 2. Battery-operated convectively-driven PCR thermal cycler.

Our key objective was the demonstration of a packaged microfluidic fuel processor with improved catalyst and integrated thermal management for waste heat recovery. To demonstrate the feasibility of a microfluidic fuel processor, we addressed several technical issues through iterative theoretical and numerical analysis, design, and development.

Our approach was to form a catalytic microchannel reactor (Fig. 1) for steam reforming of methanol. The steam reforming reaction occurs at about 300 °C. The reaction produces hydrogen and carbon dioxide, according to the reaction:



In addition to reforming, methanol also undergoes a decomposition reaction to a minor (but significant) extent, producing hydrogen and carbon monoxide according to the reaction:



The carbon monoxide produced by the above reaction tends to poison the catalyst used in the fuel cell, so its concentration needs to be reduced to well under 100 ppm with the use of a preferential oxidation catalyst, commercially available.

With adequate surface area of the catalyst material and applied heat, the microfluidic reformer produces hydrogen

Integrated Microfluidic Fuel Processor for Miniature Power Sources

R. S. Upadhye, J. D. Morse, M. A. Havstad, D. A. Sopchak

Portable power sources are important to all aspects of the military, weapons testing, and intelligence communities. New lighter-weight, longer-lasting power sources are required, with many of these having specific performance criteria for direct application. The current proton exchange membrane (PEM) fuel cells are limited to 3 to 15% methanol solution, thereby limiting their power and energy density. Our approach is to reform the methanol in a separate microreactor, converting it to hydrogen, and feed the hydrogen to the fuel cell, thus exploiting the very high energy densities of liquid fuels.

gas fuel with minimal power input to sustain the microreaction. The hydrogen and carbon dioxide byproducts (along with trace quantities of carbon monoxide and steam) are then delivered to the fuel cell manifold by microfluidic interconnects. This system approach allows for an integrated solution addressing issues of fuel storage, processing, and delivery.

In the initial phase, we used two commercial catalysts containing CuO and ZnO on Al_2O_3 . Our experiments (Fig. 2) on these catalysts show conversions ranging from 80 to 96% at temperatures between 250 and 300 °C, corresponding to 500 mW to 5 W electrical power.

We have done extensive comparisons of both simple (tubular) reactors and advanced reactors (serpentine reactors on a silicon wafer), and in all cases have

obtained reasonable or better agreement using at least one of the sets of kinetics constants available in the literature.

In addition, we have successfully synthesized and deposited CuO/ZnO catalyst on the walls of the microchannel reactor using a wash-coat process developed during the course of this project. We have also operated a PEM fuel cell fed directly by the reformat product gas to yield up to 6 W electrical power; our

goal was to reach and exceed 500 mW.

Building on ideas developed here and under another project, we have developed a thermal package that allows high thermal gradients under a geometry that makes the device suitable for use in laptop computers.

This project has already resulted in four conference presentations, with more on the way. Two publications in peer-reviewed journals are currently being prepared. In addition, three records-of-invention have been filed.

The main customer for this product in the short run is the sensors community, where long-lasting power sources are needed. Beyond that, the entire commercial sector of consumer electronics where long-lasting, light-weight power sources are desirable, constitutes the customer base.

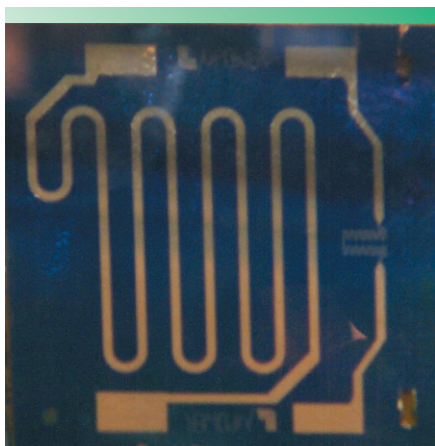


Figure 1. Photograph of the microreactor containing commercial CuO/ZnO catalyst.

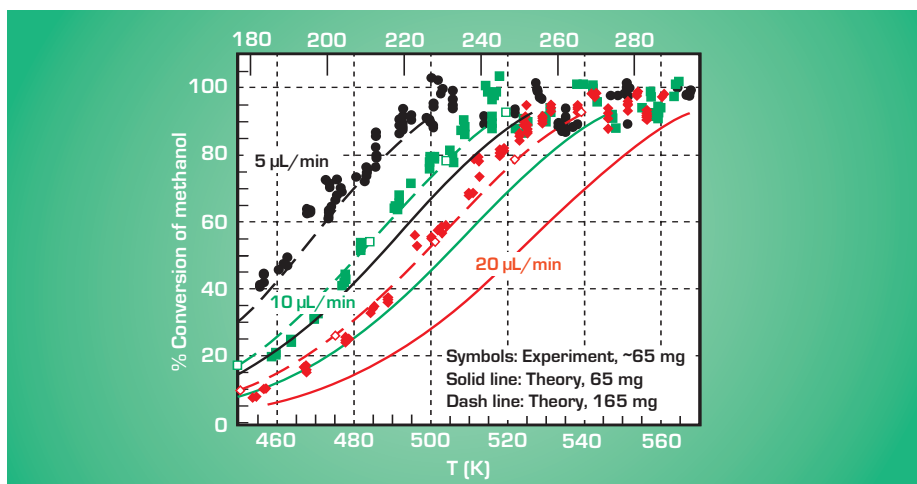


Figure 2. Conversion vs. temperature data for different flow rates.

Multiplex bioassays, capable of performing a battery of screening tests simultaneously, are critical for biodefense and medical diagnostic applications. Biomarkers composed of DNA sequences, RNA sequences, or specific types of proteins can be detected with assays based on nucleic acid hybridization or affinity-binding reactions. While tremendous advances in multiplexed biomarker analysis have come about with the advent of DNA and protein chips (microarrays), this technology is limited in several important ways: microarrays are 2-D, limiting interaction with target molecules; gene and protein chips are aimed at only one type of marker (DNA, RNA, or protein); DNA and protein chips are not reconfigurable by the user; and microarray technologies require the manufacture of specific chips, an approach that is expensive and time-consuming.

Our approach uses solution array technology within an integrated, reconfigurable microfluidic system for user-specified multiplexed biomarker assays for the early detection of disease. Solution arrays are similar to gene and protein chips, but use surface functionalized particles in solution, rather than the binding of biomolecules to a fixed surface. Instead of correlating fluorescence with location, as in a chip format, the particles are encoded for identification. Results are read by examining particles for their encoded type and for the presence or absence of the fluorescence indicative of a positive binding event.

The flexibility of solution arrays means that different types of functionalized particles can be added as desired by an end user, and particles for DNA, RNA, and protein detection can be used simultaneously in a single low-cost format.

The particles used in this project are nanobarcode (see figure), short metallic nanowires that bear patterns of light and dark stripes, analogous to the stripes in a supermarket barcode. These particles offer unique advantages in their

Microfluidic System for Solution-Array-Based Bioassays

G. M. Dougherty, F. Y. S. Chuang, S. S. Pannu, K. A. Rose

We are developing an integrated, reconfigurable microfluidic system for performing user-specified multiplexed biomarker assays for the early detection of disease using solution-array technology.

ability to be identified using standard light microscopy, avoiding the need for complicated spectroscopic or flow cytometry methods. The surface functionalization of metal particles is understood, and the nanobarcode can be made with magnetic materials, opening up new possibilities for manipulating, transporting, and trapping the particles using magnetic and electric fields.

In FY03, the first year of the project, we studied the transport behavior of nanobarcode in liquid, including their behavior in pressure-driven and electrokinetic flowfields, their sedimentation rates, orientation in suspension and on fixed surfaces, and the changes in their behavior in solutions of varying ionic content.

With data from these experiments, computer models were advanced to better predict the behavior of metallic nanowires within microfluidic systems. We also advanced the methods of surface functionalizing the nanobarcode

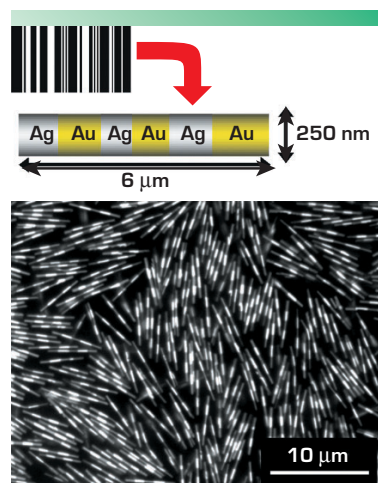
to optimize their transport behavior and their performance as substrates for biomolecule immobilization.

Antibody binding tests using our most recently developed protocol show a 10x improvement over the prior state of the art. Rapid progress has allowed us to implement an assay panel of six different immunological tests within the nanobarcode format at the end of the first year.

In parallel with the transport and bioassay development efforts, we have worked with an industrial collaborator, to further the state of the art in automated readout of nanobarcode arrays and to transition this technology to LLNL for the next stages of our project.

In FY04, we will combine the knowledge gained in the first year of the project with LLNL's expertise in polymer-based microfluidic devices to prototype components for mixing, moving, and incubating the particles, and displaying them for optical readout.

Parallel bioassay and optical image processing efforts will converge with these fluidic components to enable the demonstration of a prototype automatic, low-cost system suitable for benchtop or field use by the conclusion of the project.



Optical microscope image of nanobarcode particles. The light and dark stripes are due to alternating bands of gold and silver metal, having different reflectivities at the observation wavelength.

Design tools will be of paramount importance to reduce the costs of developing PICs. Commercial photonic design tools are currently narrowly focused on the telecommunications industry and cannot cover the range of applications necessary for PIC design. The goal of this project was to create sophisticated PIC simulation tools that would benefit LLNL missions in national security, stockpile stewardship, weapons miniaturization, high-bandwidth diagnostics, remote sensing, high-performance computing, and secure communications.

We focused on novel lasers and nonlinear devices, such as logic gates, for all-optical digital circuits and signal processing, as well as highly sensitive sensors for analog and digital operations. For instance, the Boolean logic on which computer technology is based can be realized in PICs by integrating laser gain elements with dielectric waveguides as both optical inputs and optical outputs.

We have produced a suite of codes to simulate these devices. The codes range in sophistication from a simple lumped-parameter rate-equation-based time-domain code, through 1- and 2-D transient and steady state simulations. All of these codes have been checked for consistency with one another and validated against experimental data published in the literature. All of these codes have been documented and have had manuals written for them. We have used these codes to investigate the feasibility of building PICs based on gain-quenched laser logic (see figure).

In gain-quenched laser logic, each laser is divided into a slave section and one or more control sections. Light injected into the side of the control sections reduces the gain for the output light. The idea is that when the control is turned on, the gain is reduced

Modeling Tools Development for the Analysis and Design of Photonic Integrated Circuits

T. C. Bond, J. S. Kallman, G. H. Khanaka

Photonic integrated circuits (PICs) are devices that use light (photons) rather than electrons to perform logic functions. These devices are poised to become the next generation of high-speed information processing systems. Recent advances in material processing and device engineering lead to the integration of a number of functions on single chips. Such optical chips may enable compact, low-latency, wide-bandwidth, ultrafast, secure information systems. The goal of this project was to create PIC simulation tools to benefit LLNL missions.

(quenched) enough to stop the device from lasing.

Our lumped-parameter code, QUENCH_LLNL, uses a Runge-Kutta solver to compute the time domain response of a two-segment laser logic device. We discovered that for a standard edge-emitting laser to be quenched it must be operated near threshold, the control region must be large (on the order of 80 % of the length of the device), and the input light must be much more intense than the output light (on the order of a factor of 30).

We used QUENCH_LLNL to explore the parameter space for these devices and determined that it was possible to design devices that could switch states using less input light than they output, but it was impossible to actually build them.

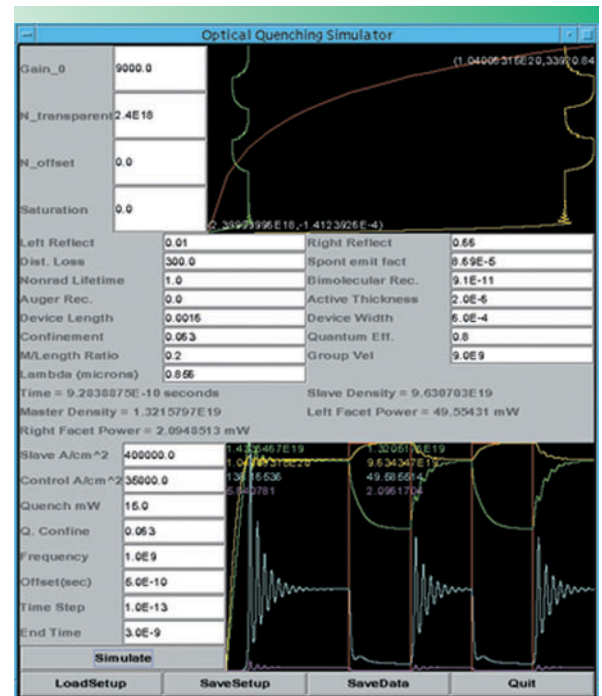
Our 1-D codes, QUENCHZ_TD and QUENCHZ_SS, were used to determine the effect that the control section position has on the switching of gain-quenched laser logic.

Although there was an effect, it was not found to be large enough to make the devices practical.

Our 2-D codes, QUENCH2D_TD and QUENCH2D_SS, were used to determine the effect of spatial hole burning and carrier diffusion on these devices. Once again, there were significant effects, but not enough to make the devices practical.

In a follow-on project described in the FY03 technology-base

reports, we began looking at nonlinear effects that could be responsible for the observed switching in experimental devices. Gain-quenching is inadequate for describing the operation of these devices.



Screen capture of the lumped-parameter code simulating a gain-quenched laser logic device. Although this simulation shows a device with good gain and reasonable speed, the device itself is infeasible to fabricate and must be run at such high currents that the device would melt, even if it could be built.

This project entails the development of advanced technologies that have potential applications to national security, such as secure, high-speed transmissions, and that will enhance LLNL's competencies in optoelectronics and high-speed communications.

By applying innovations in WDM-component technology, we are developing a compact optical CDMA (O-CDMA) encoding and decoding device that would handle large code sizes, be remotely reconfigurable by a network operator, and be compatible with commercial fiber-optic infrastructures.

The device, which comprises two indium phosphide (InP) arrayed waveguide gratings (AWG) and an array of InP phase modulators, would allow each user of a network to spectrally phase-modulate (encode) a broadband, ultra-short, transmitted optical pulse. Only the intended recipient, in possession of the correct complementary phase code, would be able to decode the transmitted information.

In FY01 and the first half of FY02, the functionality of this system was demonstrated by evaluation of a tabletop O-CDMA system. Subsequently, the effort has been focused on the fabrication of an integrated chip capable of supporting data streams within a CDMA platform. The building block of the system is the AWG, which requires complex semiconductor crystal growth and precision plasma etching.

Our design is based on InP semiconductors using the quaternary InGaAsP for the waveguide core. In FY03, we 1) designed waveguides aimed at achieving large optical confinement and low attenuation; 2) developed epitaxial crystal growth of

Reconfigurable Optical Code-Division Multiple Access for Fiber-Optic Networks

R. J. Welty, C. E. Reinhardt, N. P. Kobayashi, V. R. Sperry, I. Y. Han, E. M. Behymer, C. V. Bennett, S. W. Bond; Y. Du, S. J. Yoo (University of California at Davis)

High-speed, high-capacity fiber-optic communications networks, which allow multiple users to access the same network simultaneously by sharing the same transmission medium, have proliferated for long-distance, metropolitan, and local-area communications systems. Recently, a rapid expansion has begun into wavelength-division multiplexing (WDM) systems, which use multiple wavelengths to increase capacity. In addition, code-division multiple-access (CDMA) techniques, which were originally developed for wireless communications, can also be used to further increase the number of channels on an optical fiber.

InP/InGaAsP waveguide structures; 3) developed state-of-the-art InP/InGaAsP chlorine hydrogen dry etching (Fig. 1); 4) fabricated InP/InGaAsP AWG devices (Fig. 2) and optical modulators; 5) characterized the fabricated low-loss waveguides (loss = 1.2 dB/cm); and

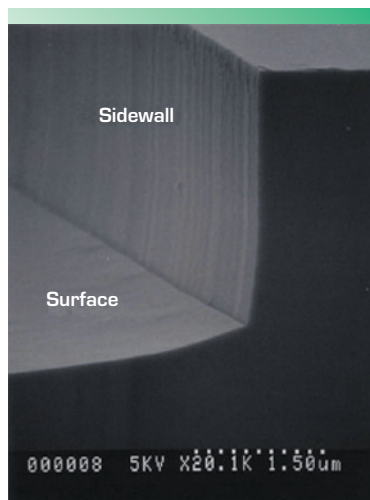


Figure 1. Scanning electron microscope photograph of InP dry-etched waveguide (cross-section) defined by electron cyclotron resonance etching. Photograph shows smooth etched surface (rms roughness of 1.0 nm) and sidewall (rms roughness of 3.7 nm).

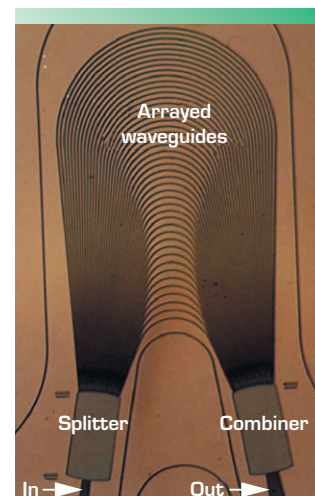


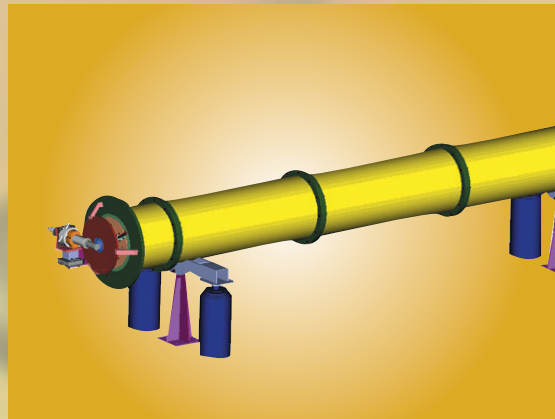
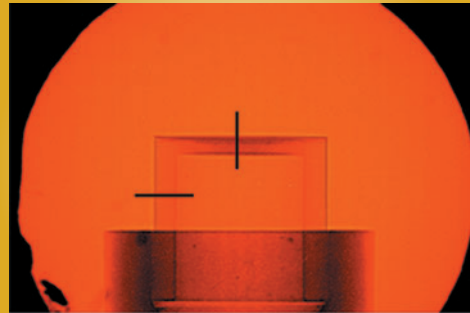
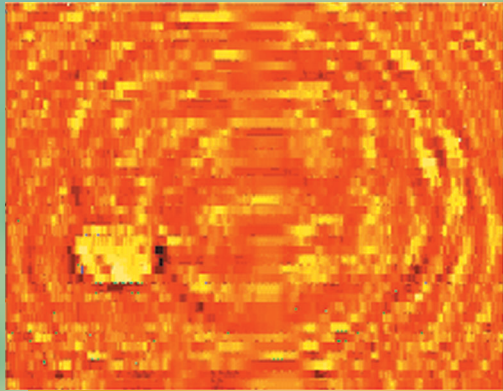
Figure 2. Photograph of fabricated AWG device. Light with many wavelengths (channels) is multiplexed from one input guide to n output guides by splitting, constructively interfering, and combining.

6) characterized the fabricated 8-channel AWG with channel spacing of 3.4 nm and signal-to-noise ratio of 20 dB.

FY03 is the last year for this project. Our exit plan began in January 2003, with the start of our DARPA-sponsored program on O-CDMA technologies, working with the University of California at Davis (UCD). UCD leads the networks simulation, coding, and architecture segment; LLNL leads the InP integrated technology development.

The foundations of the DARPA project are the discrete devices that we have fabricated for this LDRD project. The DARPA program is aimed at developing a complex semiconductor chip integrating lasers, phase modulators, waveguides, AWGs and detectors.

Center for Nondestructive Characterization



Existing approaches to threat detection have severe limitations. In general, there are trade-offs between range of detection (especially through obscurants at a distance), specificity, data-processing time, and portability.

An example on one extreme: metal detectors are fast but they cannot detect non-metallic weapons and cannot be used to monitor human threats at a distance through walls. An example on the other extreme: backscatter x rays are location-specific but cannot provide the data in real time, and are thus of no use in tactical situations. In both cases, these techniques are detecting and screening for *objects*, and do not have the capability to monitor in real time threatening actions of people through obstacles such as doors and walls.

In this project, we are researching the use of real-time FPGAs, integrated with high-resolution (cm scale), ultra-wideband (UWB) electromagnetic signals for imaging personnel through smoke and walls. Upon solving this larger-scale real-time imaging problem, we will evaluate the real-time imaging issues of detecting smaller objects, such as concealed weapons that are carried by the obscured personnel. We

Concealed Threat Detection at Multiple Frames/s

J. T. Chang, S. G. Azevedo, D. H. Chambers, P. C. Haugen, R. R. Leach, C. E. Romero, J. M. Zumstein; V. R. Algazi (University of California at Davis)

Our purpose is to investigate the science and technology necessary to enable real-time array imaging as a rapid way to detect hidden threats through obscurants such as smoke, fog, walls, doors, and clothing. The goal of this research is to augment the capabilities of protective forces in concealed threat detection.

will further examine the cognitive interpretation process of real-time UWB electromagnetic images.

While two front-end sensors can be used (acoustic and electromagnetic), we have elected to develop a beam-forming and steerable UWB array. Among other attributes, UWB has been shown to penetrate many materials (*e.g.*, wood, some concretes, non-metallic building materials, and some soils) with very high range resolution. Further, we are leveraging the LLNL UWB technical knowledge base and experiences gained through field deployments of monostatic systems. Our approach, in collaboration with cognitive sciences staff at the University of California at Davis (UCD) will be to formulate images in real time that will engage the user's vision system in a more active way to enhance image interpretation capabilities.

We have developed a numerical imaging algorithm and implemented it to study UWB beam-forming and steering. We have developed a computational simulator system to evaluate and anticipate the performance of the imaging system. It is capable of generating impulse radar images of moving targets with arbitrary trajectories, and of facilitating a parametric study of the effects of transceiver element configuration.

Figure 1 shows an image frame of a sphere target as determined from the simulator. Figure 2 shows the measured psychometric functions of different types of targets.

We have also been characterizing the existing hardware to aid us in designing the simulator to reflect the most realistic and desired performance characteristics. The preliminary results have been very encouraging and indicate that the project continues to be on track.

Figure 3 shows an image frame of a circular plate target from the laboratory system. We continue to reach out to potential sponsors and customers within both LLNL programs and external agencies.

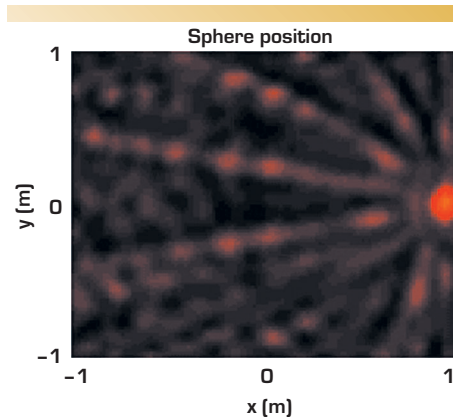


Figure 1. Simulated radar image frame of a spherical target taken by 7-transmitter, 1-receiver circular array. The target is 30-cm outer diameter and 1-m down range, and is located at the edge of the detection field of view (1 m, 0 m).

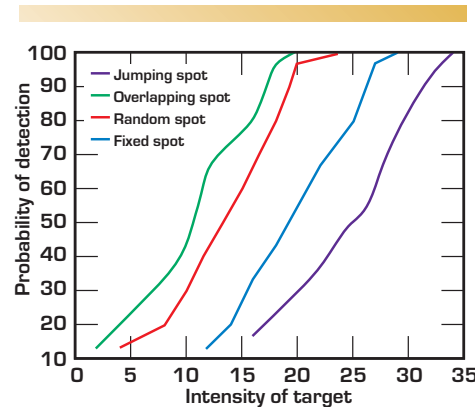


Figure 2. Measured psychometric functions of different types of targets. These are measurements of probability of detection as a function of target intensity.

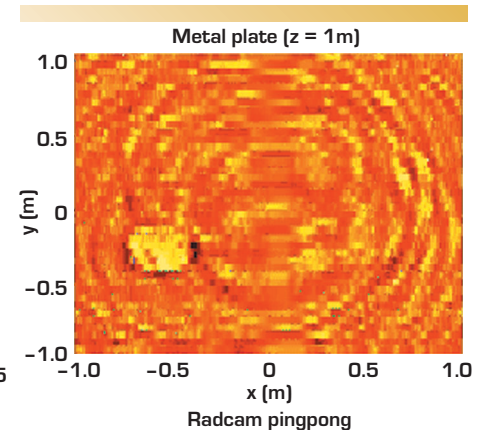


Figure 3. Laboratory-acquired radar image frame of circular metal plate target taken by 7-transmitter, 1-receiver circular array. The target is 30-cm outer diameter and 1-m down range, and is located at the edge of the detection field of view (-0.5 m, -0.25 m).

X-ray microscopy is one technique that holds promise for characterizing the internal structure of target assemblies. Sub- μm spatial resolution has been demonstrated using a synchrotron x-ray source, but that approach does not accommodate our requirements for a high-throughput and low-cost approach for characterizing production quantities of target assemblies.

This project is funding the research and development of an x-ray microscope that uses a replicated multilayer Wolter optic. The fabrication of the optic is the key to the success of this project. The replication technique coats a super-polished mandrel with reflective multilayer materials. The multilayers are covered with a 1- to 2-mm-thick layer of nickel to provide structural rigidity. The Wolter optic (multilayers with a nickel substrate) is then separated from the mandrel. This results in an optic with nearly the same figure and roughness as the mandrel. If successful once assembled and tested, this prototype microscope will provide high-throughput and high-resolution x-ray imaging of target assemblies in a laboratory setting. Moreover, this prototype would bring a new capability to LLNL that

High-Accuracy X-Ray Imaging of Mesoscale Targets

W. W. Nederbragt, T. W. Barbee, J. L. Klingmann,
C. Vargas, H. E. Martz

High-energy-density (HED) experiments play an important role in corroborating the improved physics codes that underlie LLNL's Stewardship mission. Conducting these experiments will require not only improvement in the diagnostics for measuring the experiment, but also in the fabrication and characterization of the target assemblies. Specifically, a radical improvement is needed in characterizing the target assemblies (mm-sized components with μm -sized features).

can be used in a variety of mesoscale characterization areas.


This project began in FY01. During the past twelve months, we have replicated several test optics using low-cost mandrels, and we replicated one developmental optic using our super-polished high-accuracy mandrel (see figure). We have also designed and partially constructed the prototype microscope (see figure).

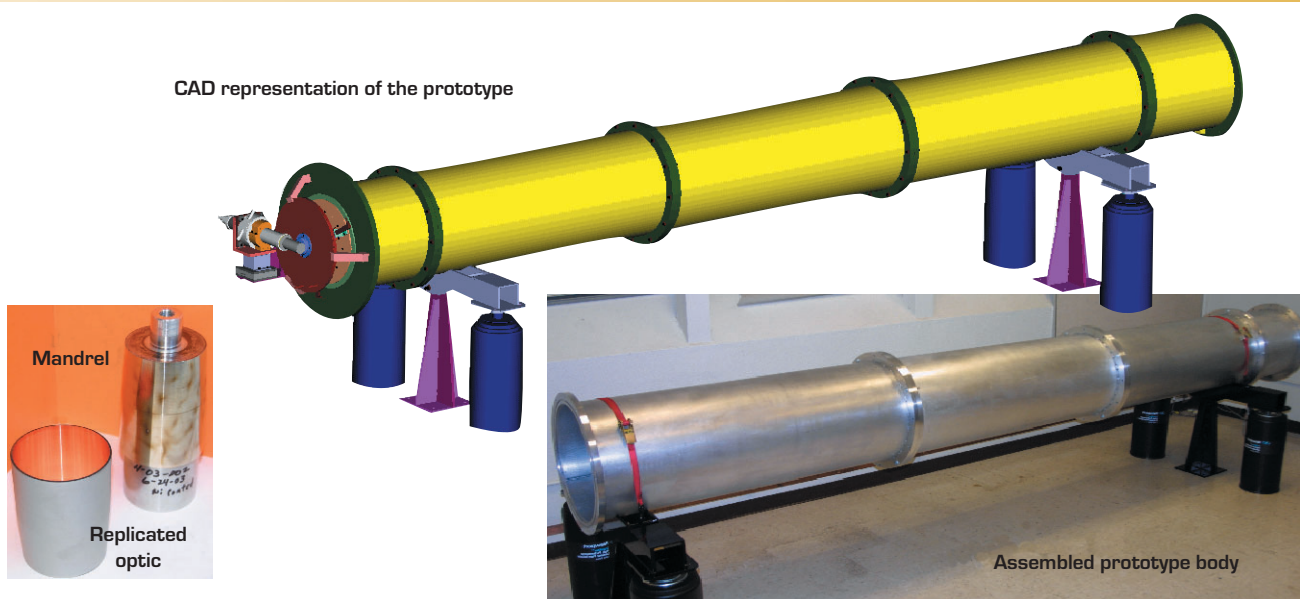
The microscope prototype consists of four major parts: the optic and target-positioning hardware; the imaging system; the x-ray source hardware; and the prototype body. The prototype body is essentially a large aluminum tube that is supported by isolators. This design provides high rigidity and good vibration isolation at a minimal cost. The x-ray source is a standard copper-anode tube source.

It is positioned via three translation stages and one rotation stage. A water-cooled shield is placed between the source and the prototype body to minimize heat transfer.

The imaging system uses a scintillator to convert the x rays to visible light, which is imaged with a CCD camera. This hardware sits on an automated positioning system with three degrees of freedom.

The optic and target-positioning system is the most complicated part of the prototype. The target is positioned via a custom-built parallel mechanism that uses flexures to provide rigidity with very little friction. The optic and target are mechanically aligned using tightly toleranced parts. This approach will minimize alignment problems during the testing of the prototype.

This project will continue as we manufacture more parts; assemble the prototype microscope; fabricate additional optics using super-polished mandrels; and test the microscope using phantoms (test parts) and real target assemblies. Ideally, this prototype will lead to the construction of a production microscope in the near future. 



X-ray microscope design and construction.

IVUS systems form images of the medium surrounding the probe based on ultrasonic scans, using a straight-ray model of sound propagation. Our achieved goal was to develop a wave-based imaging algorithm using diffraction tomography techniques.

Given the hardware configuration and the imaging method, we refer to this system as "radial reflection diffraction tomography." We considered two hardware configurations: a multimono-static mode, using a single rotating transducer, and a multistatic mode, consisting of a single transmitter and an aperture formed by multiple receivers. In this latter case, the entire source/receiver aperture rotates about a fixed axis.

Practically, such a probe is mounted at the end of a catheter or snaking tube that can be inserted into a blood vessel, part, or medium, with the goal of forming images of the plane perpendicular to the axis of rotation. We derived an analytic expression for the multimono-static inverse, but ultimately used a Hilbert space inverse wave (HSIW) algorithm to construct images using both operating modes.

Applications include improved IVUS imaging, bore-hole tomography, and nondestructive evaluation of parts from existing access holes.

A trade-off must be made between the number of transducers used and the quality of the reconstructed image. Ideally, an aperture consisting of a 360° annular array would yield the best image. Practically, it is currently not possible to construct such a fully wired array in a 0.25-mm IVUS probe, for example. Thus, we have studied rotating sub-apertures and compared reconstruction results to the single multimono-static configuration.

When operating in a reflection mode, the imaging mathematics dictates that spectrally wideband pulses must be used. The resolution of the reconstructed image is directly proportional to the number of frequencies used in the reconstruction. Under the

Radial Reflection Diffraction Tomography

S. K. Lehman, D. H. Chambers

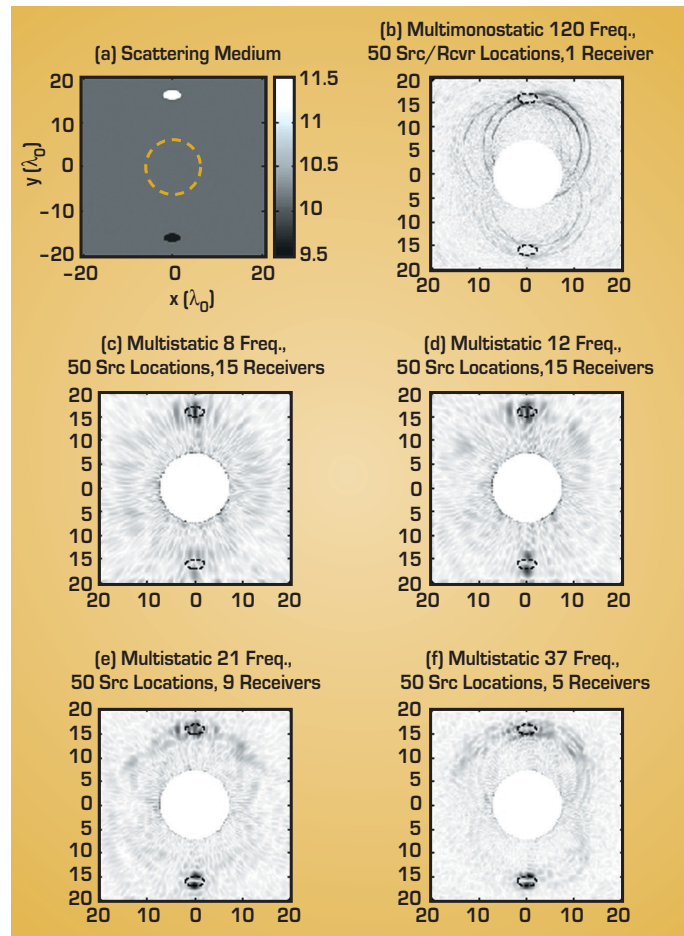
We developed a wave-based tomographic imaging algorithm based on a single rotating radially-outward-oriented transducer. At successive angular locations at a fixed radius, the transducer launches a primary field and collects the backscattered field in a "pitch/catch" operation. The hardware configuration, operating mode, and data collection method is identical to that of most medical intravascular ultrasound (IVUS) systems.

HSIW algorithm, however, increasing the number of frequencies and transducers increases the complexity of the reconstruction, the size of the intermediary data files, the reconstruction time, and the computer memory requirement. Thus, the trade-off between computer resources and resolution must also be considered.

We studied these issues using LLNL's E3D acoustic/elastic wave propagation and scattering code. We simulated a medium with two scattering objects whose acoustic properties varied from 5% below the background to 15% above it. An example of the medium is shown in the figure (a). The dashed outline indicates the location of the radial reflection probe. We performed five simulations with the configuration shown in figure (a). The reconstructed images are presented in (b) through (f). The dashed outlines superimposed on the images indicate the locations of the scatterers. Our conclusion, based upon observation of the reconstructed results, is that a single transducer

offers insufficient spatial diversity to localize the object azimuthally. As can be seen in the multimono-static reconstruction of (b), the concentric arcs indicate there is an azimuthal ambiguity resulting from the lack of spatial receiver diversity. This is a result of off-radial axis scattering

that is not collected by the transducer. Improved azimuthal localization is achieved as more receivers are included; however there is a loss of range resolution as fewer frequencies are included in the reconstruction. In summary, scatterer azimuthal resolution improves as more receivers are used; and range resolution improves as more frequencies are used.



(a) Homogeneous medium with two scattering objects. (b) Multimono-static reconstruction. (c) – (f) Multistatic reconstructions in which the number of elements in the aperture and number of frequencies used were varied as indicated.

In the area of amplitude contrast, we have focused on two x-ray microscopes, one 8 keV, the other 59 keV.

The mechanical design of the 8-keV prototype microscope is nearly complete. Several replicated optics have been fabricated for testing. The first developmental Wolter optic was fabricated. The optic quality will be determined in FY04. The prototype is being assembled.

We have preliminary designs for a 59-keV prototype instrument. After carefully considering all system requirements and performing coarse optimizations, we have determined that the detector will drive the final design. Unlike the lower energy 8-keV microscope that can use several different types of detectors, there are few options for efficiently detecting hard x rays at the requisite spatial scales needed to ultimately achieve sub-micrometer performance. After verifying that our proposed solution [coupling highly-collimated scintillator screens directly to a CCD] meets our specification, we will finalize the design of the 59-keV prototype microscope.

We have made progress also in algorithms for object recovery. We are fully

Tabletop Mesoscale Nondestructive Characterization

H. E. Martz, M. B. Aufderheide, T. W. Barbee, A. Barty, H. N. Chapman, J. A. Koch, B. J. Koziolowski, W. W. Nederbragt, D. J. Schneberk, G. F. Stone; M. Pivovarov (University of California at Berkeley)

We have made significant progress in the area of research and development of tabletop mesoscale nondestructive characterization. Our FY03 accomplishments include completion of projects in amplitude contrast, algorithms for object recovery, phase contrast, and modeling.

exercising laminographic and conjugate gradient iterative object recovery techniques. This includes further developing our simulation capability. From sequences of translated simulated images we are exploring algorithms that may identify boundaries of images at various planes.

We have also investigated the use of phase-contrast imaging techniques in both the point-projection geometry and in the Wolter optical system. Numerical modeling of a variety of objects indicates that phase contrast features have a significant effect on the collected image for a range of objects of interest. We modeled KCAT point projection imaging of a Be-shock tube (Fig. 1) and polyethylene surrogates, including for the first time the effects of phase contrast, and explained the bright edges observed in previously collected data. Partially

x-ray illumination for phase contrast of this feature.

As one of our modeling accomplishments, we have built HADES input decks that model recently fabricated cylindrical and spherical reference standards. These images were generated with HADES using LLNL's Evaluated Photon Data Library, and are simply attenuation projections. We are developing a new version of HADES that will also compute optical path difference (phase) projections using form-factor tables from the Center for X-Ray Optics at the University of California at Berkeley. These quantities are the raw materials for use in post-processing simulations of phase-contrast microscopy. We have worked out plans for including this new physics in HADES, but the code has not yet been written.

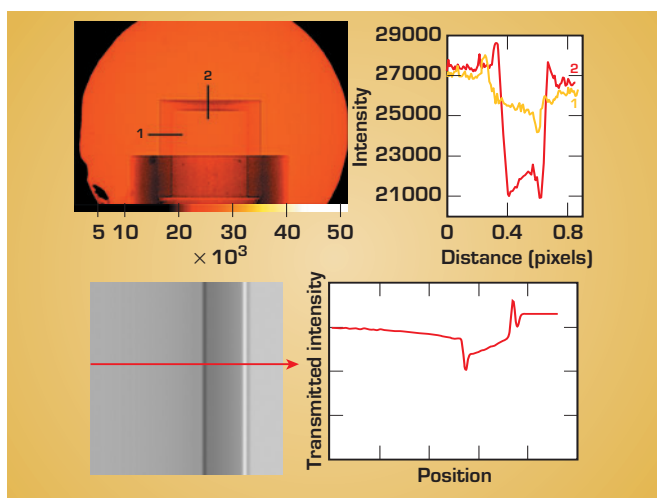


Figure 1. Top: KCAT point projection image at 50 kV of a hollow Be cylinder with a cap. Bottom: Calculated Fresnel-Kirchoff scalar diffraction theory results of the Be cylinder.

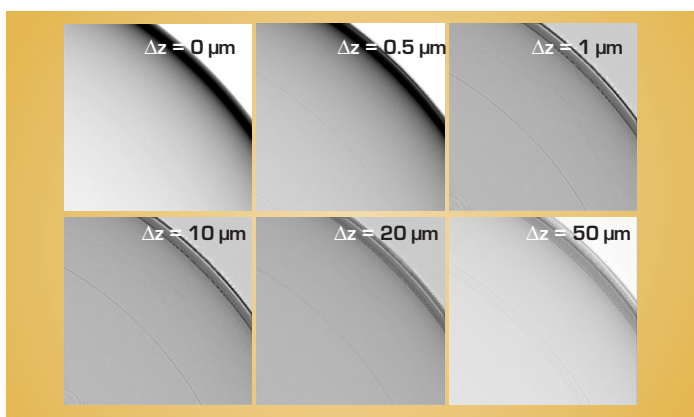


Figure 2. Phase contrast images of a D/T ice boundary obtained by transport-of-intensity defocus method using disk source and full Wolter aperture, where Δz is the position of the object from the object plane center. Phase enhanced images at Δz of 0.5 to 20 μm reveal the D/T ice boundary not observed in amplitude contrast images, $\Delta z = 0 \mu\text{m}$.

Inspecting multilayered structures with a guided wave relies on exciting modes with sufficient energy in the layer of interest and on the surface. Suitable modes for inspection must be determined. We are developing a new method of phasing an array to search the dispersion space for guided wave modes suitable for inspecting inaccessible areas of multilayered structures. This project is developing a model and experimental hardware to preferentially excite guided acoustic waves to characterize multilayered structures.

We are also developing phased-array methods for beam-steering and focusing of bulk waves for the nondestructive evaluation (NDE) of multilayered structures for accessible areas. We are extending array technology from a single layer into multilayered media. This requires reconstruction algorithms to be modified to account for refractions at interfaces and changing wave speeds in different layers.

During FY03, for guided waves we designed and built the electronics hard-

Ultrasonic NDE of Multilayered Structures

M. J. Quarry, K. A. Fisher, J. Rose (Pennsylvania State University)


Several programmatic applications require the inspection of multilayered structures with barriers to placing sensors in the area of concern. This prevents the use of many traditional nondestructive techniques. Inspection without disassembly is currently not possible. This project is developing two technologies for inspection: 1) ultrasonic guided waves, a potential method for sending sound into inaccessible areas to characterize the integrity of embedded parts; 2) bulk-wave-array technology, which can focus sound at an arbitrary point without scanning or submersing the system in water. The inspection techniques developed in this work will enhance LLNL's role of stockpile stewardship.

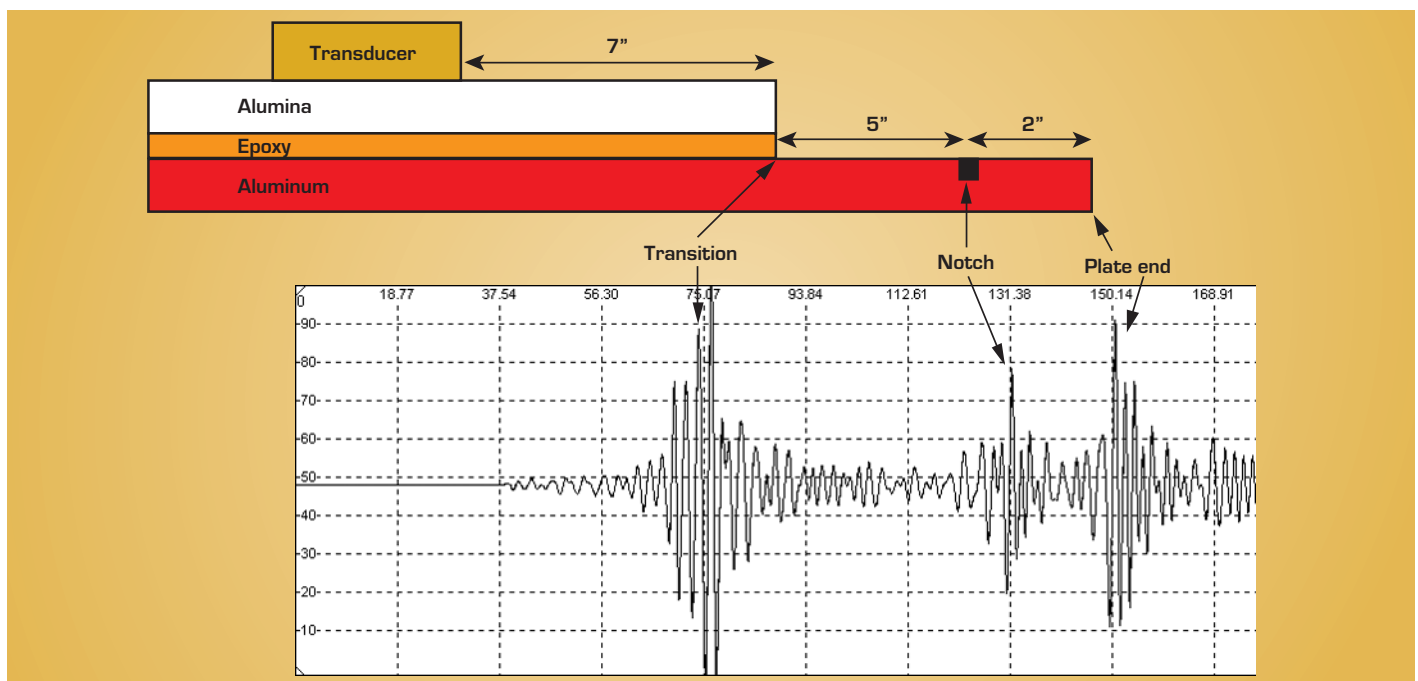
ware to synthetically phase an array; combined a dispersion model with our source model to calculate a simulated RF waveform; and demonstrated the detection of a notch in a multilayered structure. For bulk waves, a beam-forming reconstruction algorithm was modified for imaging. A void in an acrylic-epoxy-lexan structure was successfully imaged using the modified reconstruction algorithm.

Electronics capabilities were developed to synthetically phase an array with an accuracy of 10 ns. A tone-burst pulser was added to the system to

enable pulse widths of up to 200 ms, which produces a narrower band of frequency excitation. The new pulser also enables weighted windowing of the pulse to reduce side lobes in the frequency spectrum. The new electronics will result in improved signal-to-noise.

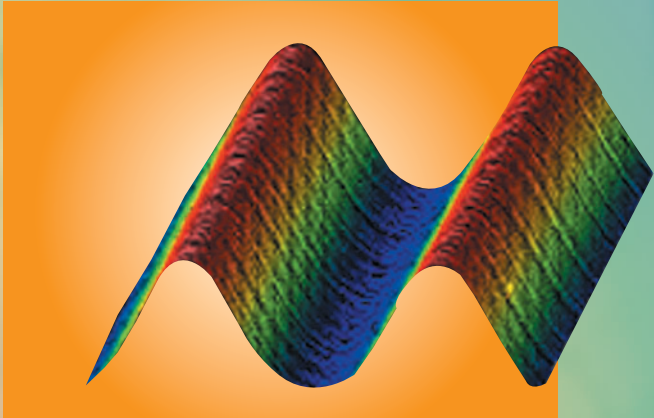
The technique of sweeping the dispersion space to determine suitable modes of inspection for a multilayered structure was demonstrated on an alumina-epoxy-aluminum structure. A notch was placed in the bottom aluminum layer and detected, as shown in the figure. A paper detailing our work was accepted for publication in a peer-reviewed journal.

In FY04, we will perform experiments on multilayered structures with surrogate materials for challenging characterization applications. We will construct improved arrays with feedback from modeling and experimental results. Feasibility studies will be conducted on programmatic-like structures. 



Sample RF waveform showing detection of a 1-mm-deep (30% through-wall) notch with a 1-mm-x-25-mm cross-section in an alumina-epoxy-aluminum multilayer structure with a guided wave mode.

Center for Precision Engineering



This project developed a 2-kHz rotary FTS capable of 50- μm PV motion at low speeds, and 5- μm PV sinusoidal motion at 2 kHz. Figure 1 is a photograph of the system. We have demonstrated 2.5- μm PV at 2 kHz, producing 20 g's tool tip accelerations, while diamond turning an optical quality surface on a workpiece (Fig. 2).

The aluminum workpiece in Fig. 2 has an outer diameter of 9 mm and 250 radial grooves on the face that were machined at 480 RPM. Tracing a profile along the face, along any fixed radius, the grooves describe a sinusoidal waveform with 2.5- μm PV amplitude and a spatial wavelength ranging from 110 μm at the outer diameter to 30 μm at the inner diameter. Figure 2 also shows optical measurements of the surface. The measured roughness along a groove [across the feed marks] is better than 12 nm rms.

High-Bandwidth Fast Tool Servo for Single-Point Turning High-Energy-Density Physics Targets


R. C. Montesanti, J. L. Klingmann;
D. L. Trumper (Massachusetts Institute of Technology)

High-energy-density experiments play an important role in corroborating the improved physics codes that underlie LLNL's stockpile stewardship mission. Single-point diamond turning has been the best method for producing accurate, optically smooth surfaces on target components, but new experiments require surfaces that exceed LLNL's current capability. A fast tool servo (FTS) is a small, fast-moving machine axis which, when added to a single-point turning machine, will provide LLNL the capability to fabricate these more complicated target surfaces.

It should be noted that the environment housing the diamond turning machine used to produce this part is less than ideal for producing optical quality surfaces because of the close proximity of heavy rotating machinery (e.g., compressors) and poor thermal control. Lower surface roughness values should be achievable in a more controlled environment.

Closer examination of the "sinusoidal" profile in Fig. 2 reveals a departure from a pure sine wave. Note that the peaks are slightly sharper than the valley. The addition of adaptive feed-forward cancellation control techniques is expected to reduce the following error of the tool tip, thus allowing the production of higher accuracy surface topographies.

Continuing work has already begun on the design of a new 10-kHz rotary FTS that will use a novel variable-reluctance actuator capable of a ten-fold increase in actuator force density, with a planned tool tip acceleration of 1000 g's. The 10-kHz FTS will have a maximum stroke of 50- μm PV.

FY04 activities will focus on developing, building, and testing the new 10-kHz system, and developing advanced controller techniques for improving trajectory following. 

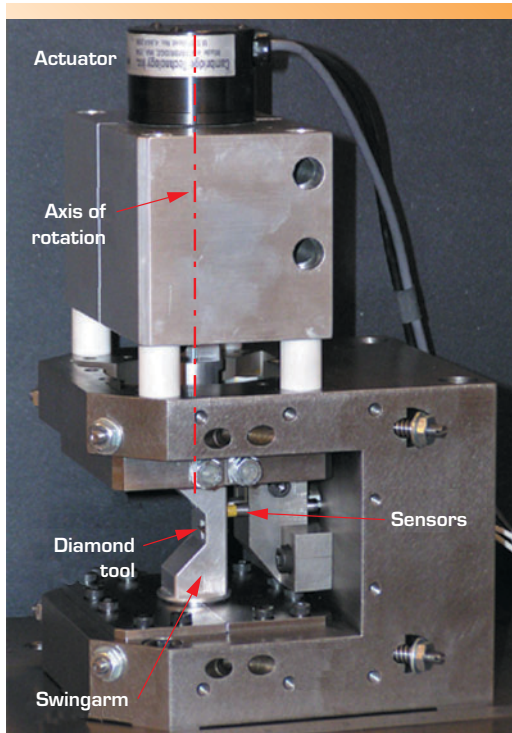


Figure 1. 2-kHz rotary fast tool servo.

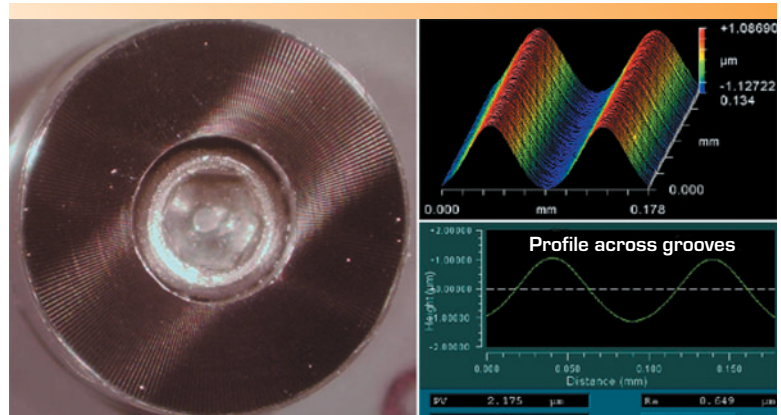
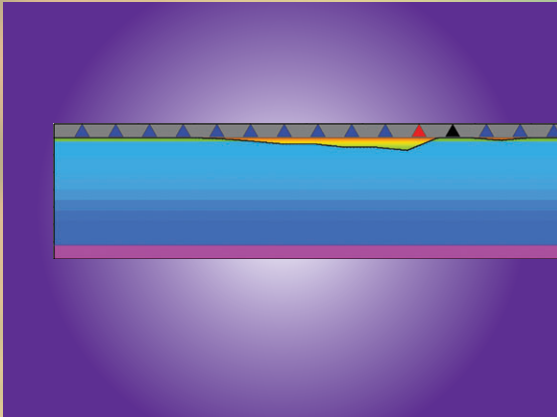
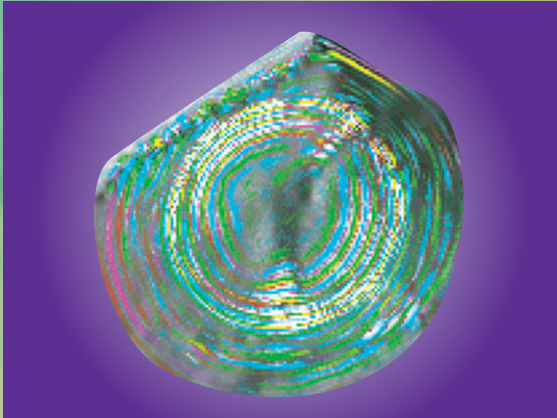


Figure 2. (Left) Diamond-turned workpiece with 250 radial grooves on the face. (Right) 3-D surface map of a section of two grooves (upper), and profile across the grooves (lower). Profile along a groove (not shown) reveals 11.6 nm rms surface roughness.

Center for Complex Distributed Systems



Our goal is to investigate two critical technologies for achieving security in the containerized shipping industry: 1) a radiation sensor that must be extremely low power (<100 μ A); and 2) a communications network that has similar power requirements and forms an ad hoc network of thousands of nodes (containers) in an extreme multipath environment.

These two areas are the key missing R&D components in support of a system concept (see Fig. 1) that would detect WMDs entering the country in shipping containers, *before* arriving at U. S. ports, and without impeding trade flow. The sensors must be inexpensive and permanently mounted (10-year lifespan).

The overall project will produce two key results. The first is a new radiation sensor concept that can integrate the radiation over time (it takes seven days to cross the ocean), has limited discrimination of energy bands, and is low in power draw. The leading candidate is a set of dosimeters (either thermoluminescent (TLDs) or optically stimulable) that have varying amounts of shielding to crudely measure spectral content, and are remotely read, then reset.

The second result will be a new communication technique for networking tens of thousands of sensors (as is likely on a large ship) using energy-efficient signaling and routing protocols. The sensors must be queried and the data extracted by multiple hops to the ship's infrastructure, using very low power levels (sub-milliwatt). Such scalable ultra-low-power networks have never before been accomplished.

In this first year of the project, we have studied possible radiation detection sensors; performed several measurement studies of TLDs and advanced neutron detectors; measured background radiation on two container ships; performed radio frequency propagation studies on board two ships (see Fig. 2); and are developing low-power communications and networking protocols.

Cargo Container Security Sensor System

S. G. Azevedo, K. E. Sale, B. D. Henderer, C. L. Hartmann-Siantar, J. Lehmann, L. S. Dauffy

Security of the containerized shipping industry with respect to the trafficking of weapons of mass destruction (WMD) will be achieved with "smart containers" of the future. We have investigated smart containers with embedded, permanent sensors and communications subsystems.

Measurements of radiation levels from a known source in a shipping container compared well to simulated results for various scenarios. These measurements have led to an initial design for the coming year. The RF experiments pointed out the need for an ultrawideband (UWB) physical implementation of the communications system, while the networking research has produced a new energy-efficient protocol mechanism. We have

also initiated publications describing our work and results.


Our project will strengthen homeland security by researching and developing a sensor system concept to detect WMD components entering the U. S. in shipping containers. Furthermore, both the sensor and networking aspects of this project have relevance to other national needs in the military and intelligence fields. DOE/NNSA projects for long-term storage of radioactive substances with small low-cost sensors will also benefit from this research. The exit plan calls for deployments through DOE/NNSA, as well as through other government agencies such as the Departments of Commerce, Transportation, Homeland Security, and Border States. 



Figure 1. Conceptual drawing of a "container ship of the future" that has low-cost sensor packages in every container. Each measures the distributed radiation environment and communicates results to authorities. Clustered anomalies will trigger inspection.



Figure 2. LNL team members on board a container ship (APL President Wilson) measuring background radiation and electromagnetic propagation at various ship locations above and below deck.

The goal of this project is to build capabilities in acquisition system design and application, and in full 3-D finite-difference modeling, as well as statistical characterization of geological heterogeneity. Such capabilities, coupled with a rapid field analysis methodology, based on matched-field processing, are applied to problems associated with surveillance, battlefield management, detection of hard and deeply buried targets, and portal monitoring. This project benefits the U.S. military and intelligence communities in support of LLNL's national security mission.

FY03 was the final year of this project. In the two and a half years this project has been active, numerous and varied developments and milestones have been accomplished. A wireless communication module was developed to facilitate rapid seismic data acquisition and analysis. The E3D code was enhanced to include topographic effects. Codes were developed to implement the Karhunen-Loeve (K-L) statistical methodology for generating geological heterogeneity that can be used in E3D modeling. The matched-field processing methodology applied to vehicle tracking, and based on a field calibration, to characterize geological heterogeneity was tested and successfully demonstrated in a tank tracking experiment at the Nevada Test Site (NTS). A 3-seismic-array vehicle tracking

Developing Smart Seismic Arrays

P. E. Harben, D. B. Harris, S. C. Myers, S. C. Larsen,
J. L. Wagoner, J. E. Trebes, K. E. Nelson

Seismic imaging and tracking methods have intelligence and monitoring applications. Current systems, however, do not adequately calibrate or model the unknown geological heterogeneity, nor are they designed for rapid data acquisition and analysis in the field. This project seeks to build the core technological capabilities, coupled with innovative deployment, processing, and analysis methodologies, to allow seismic methods to be used effectively in seismic imaging and vehicle tracking where rapid (minutes to hours) and real-time analysis is required.


testbed was installed on site at LLNL for real-time seismic tracking methods. A field experiment was conducted over a tunnel at NTS that quantified the tunnel reflection signal and, coupled with modeling, identified key requirements in experimental layout of sensors.

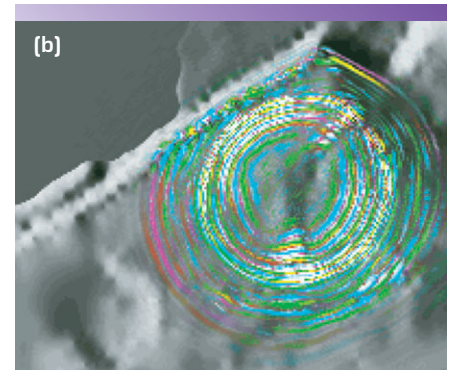
A large field experiment was conducted at the Lake Lynn Laboratory (Fig. (a)), a mine safety research facility in Pennsylvania, over a tunnel complex in realistic, difficult conditions. This experiment gathered the necessary data for a full 3-D attempt to apply the methodology, and to analyze the capabilities to detect and locate in-tunnel explosions.

In FY03 specifically, a large and complex simulation experiment was conducted that tested the full modeling-based approach to geological characterization using E3D, the K-L statistical methodology, and matched-field processing applied to tunnel detection with surface seismic sensors. The simulation validated the full methodology and the need for geological

heterogeneity to be accounted for in the overall approach. The Lake Lynn site area was geologically modeled using the code Earthvision to produce a 32-million node 3-D model grid for E3D (Fig. (b)).

Model linking issues were resolved and a number of full 3-D model runs were accomplished using shot locations that matched the data. E3D-generated wavefield movies showed that the reflection signal would be too small to be observed in the data due to trapped and attenuated energy in the weathered layer. An analysis of the few sensors coupled to bedrock did not improve the reflection signal strength sufficiently because the shots, though buried, were within the surface layer, and hence attenuated. Ability to model a complex 3-D geological structure and calculate synthetic seismograms that are in good agreement with actual data (especially for surface waves and below the complex weathered layer) was demonstrated. We conclude that E3D is a powerful tool for assessing the conditions under which a tunnel could be detected in a specific geological setting.

Finally, the Lake Lynn tunnel explosion data was analyzed using standard array-processing techniques, with the result that single detonations could be detected and located but simultaneous detonations would require a strategic placement of arrays. 



(a) Surface seismic shot detonation at the Lake Lynn site during field experiment. (b) Map view of the surface wavefield potential calculated by E3D for (a). P-waves are magenta; S-waves are turquoise. Simulations verify that advanced signal processing methods are required to detect and image underground facilities.

Sedimentary basins can result in significant amplification of ground motions and accurate simulations must be capable of representing basin effects. We investigated the application of this model in a case study application to a region in Southern Nevada, encompassing the Nevada Test Site (NTS) and the Las Vegas Valley. We used historical recordings of NTS nuclear explosions and recent earthquake recordings to constrain ground motion response and basin structure. We simulated low frequency (<1 Hz) ground motion in Las Vegas Valley with the elastic finite-difference code. We demonstrated that the relative amplification, as well as some of the complexity in the waveforms can be predicted.

A model of the basin depth was derived from gravity data in an independent published study, while a model of compressional velocity structure of the basin was derived from seismic refraction studies. We used historical accelerometer data, as well as newly acquired broadband teleseismic data to measure

Evaluating a Regional Simulation Model for Seismic Wave Propagation

H. Tkalcic, A. J. Rodgers, D. B. McCallen

A finite-difference-based, elastic wave propagation model has recently been developed for simulating surface ground motions generated by propagating seismic waves.

basin response and evaluate these models. Delay times of teleseismic P-waves show variation of up to 0.5 s across relatively short distances (15 km or less), providing constraints on basin structure. Teleseismic P-waves have favorable signal-to-noise for low frequencies (0.1 to 1.0 Hz). These data provide complementary site response measurements to those obtained from earthquakes and NTS explosions. Our results indicate an amplification factor of 5 for the basin sites relative to "hard" rock sites.

To understand the sensitivity of ground motion to basin structure we took a 2-D "slice" through a complex 3-D structural model of Las Vegas Valley, including laterally varying basin depth. We investigated the effects of various model features on

estimated ground motion, including sedimentary velocity profiles and shallow (≤ 50 m) velocities. Figure 1 shows an illustrative model and demonstrates the influence of the basin structure on the seismic data.

We investigated the sensitivity of the amplification observed at the basin sites by varying the shear and compressional velocities and density in a 50-m-thick surface layer of the basin. In Fig. 2, we illustrate the difference between a basin and a rock site (red and black in Fig.1), for a series of runs, for shear velocities of 500 m/s to 1500 m/s, with a step of 250 m/s in the shallowest 50 m.

Although we cannot produce the same amplitude as in the real data due to the 2-D approximation, we can compare the relative amplification between the two stations, for different values of elastic parameters. Decreasing the surface shear velocity clearly affects the amplitude, as well as the duration of the actual ground motion. Our comparison of theoretical and observed site response indicates that the properties of the thin surface soil layer significantly effect the observed surface motions.

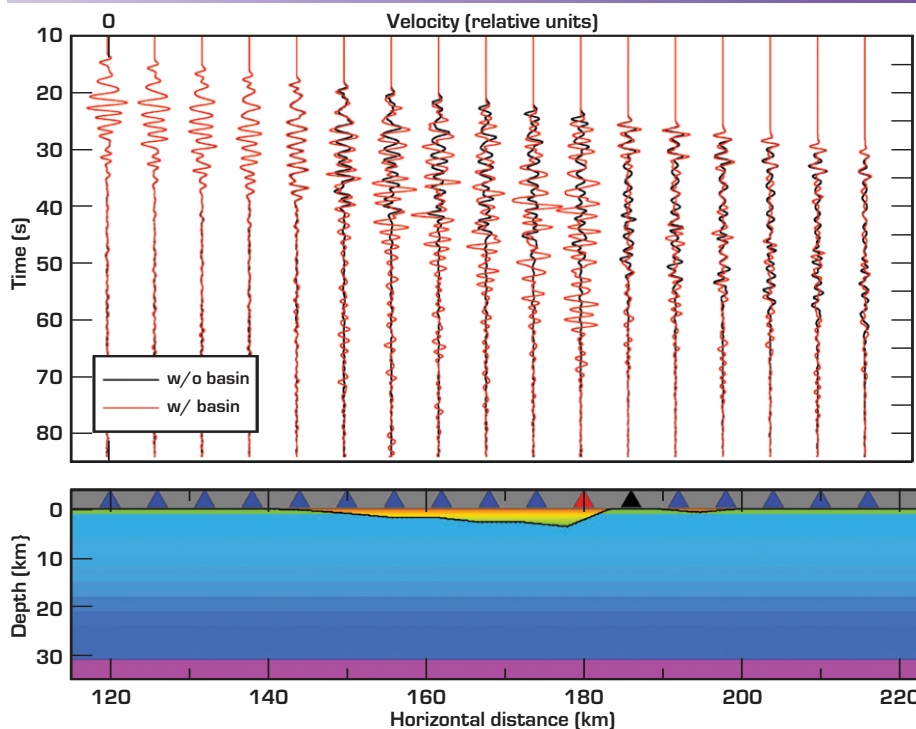


Figure 1. Two-dimensional wave propagation simulations to investigate basin amplification. Top: theoretical seismograms for models with (red) and without (black) basin. Bottom: physical model showing seismic velocity structure.

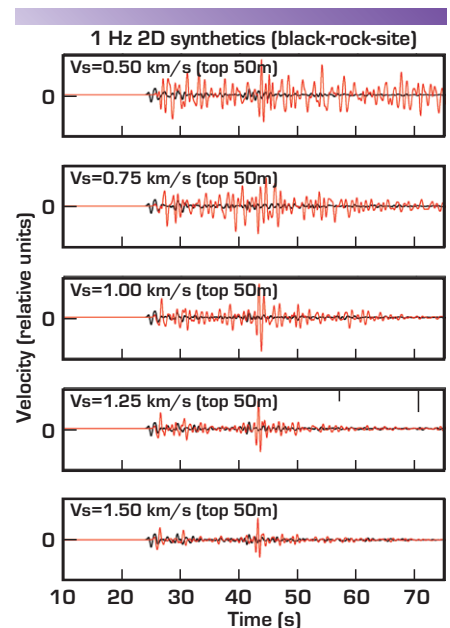


Figure 2. The effect of low shear velocity sediments.

Intelligence operations require short-range wireless communications systems capable of collecting data rapidly, and transmitting it covertly and reliably. Such systems must be robust; have a low probability of detection and intercept; employ low-power, small-size hardware; and interface easily with other systems for analysis or to establish long-distance links. Commercial communication systems that operate in fixed-frequency bands are easily detectable and are prone to jamming, among other shortcomings.

We have been focusing on the three key operational modes for DoD and the intelligence community: 1) secure sensor and voice communications over a 1-km range; 2) ground-to-ground and air-to-ground data channels for small, unmanned air vehicles; and 3) network communication for large numbers of sensors in a local area, including multi-path and extremely low-altitude operations.

The goals of this project are to develop and demonstrate 1) UWB communication with a capacity of 5 Mbps and a range of 1 km; 2) multi-channel capability with sensors; 3) a testbed for application development; and 4) performance standards for bit error rate and low probabilities of detection and intercept.

In FY03, we have refined our UWB communication transceivers for voice, video, and digital-data communications for intelligence applications (see figure). We have performed modeling and propagation analyses and developed 1) a UWB radio and bit error (BER) boxes with a capacity of 1 Mbps, a range of 100 m, and a power requirement of < 0.5 W; 2) a MATLAB graphical user interface for our models; 3) an interface for real-time applications; and 4) a network and architecture design and implementation.

Radio networking was one of the main objectives of our FY03 work. We

Ultrawideband Communications


F. U. Dowla, A. Spiridon, D. M. Benzel

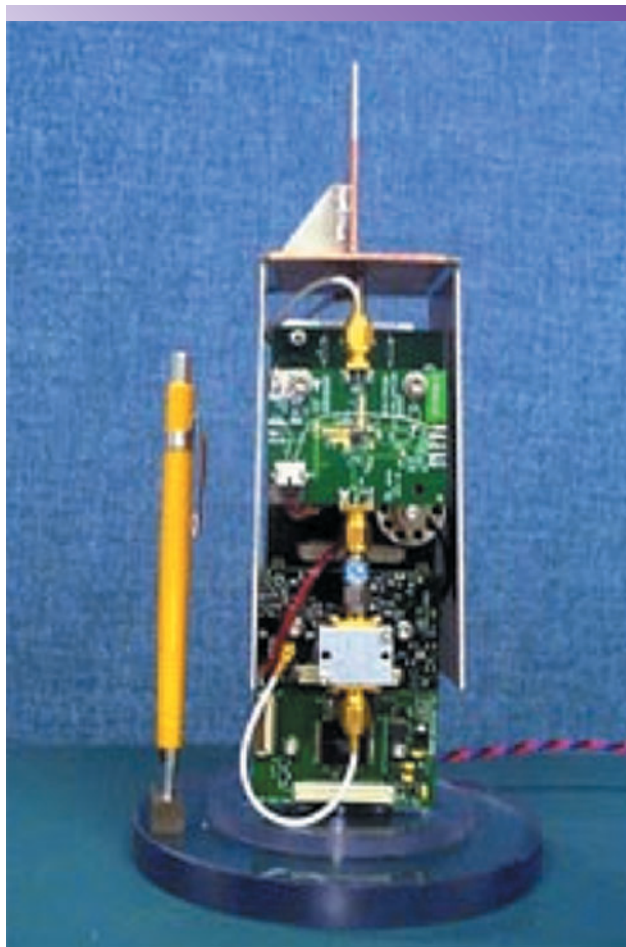
We have built an ultrawideband (UWB) radio for our compact sensor node. The sensor node is also equipped with an antenna, global positioning system (GPS), UWB radar, micropower impulse radar (MIR), processing unit, and batteries. Network protocols were developed to interface with our UWB radio design. Sensor radio nodes of this type will play a critical role in modern wireless sensor networks for intelligence and battlefield applications.

have completed and tested UWB radios for star networks and a mesh network with UWB repeater nodes. The features of the mesh network include flood routing; unidirectional communication; and redundant transmission, with media access control by pseudo-slotted, fixed, re-transmission back-offs. These provide

a very wide set of network protocols for increasing the range of our point-to-point UWB transceivers many times.

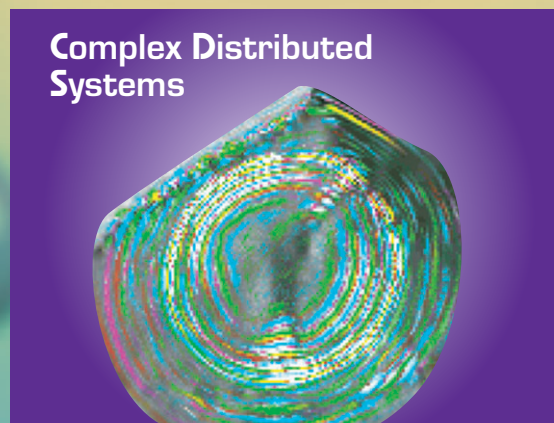
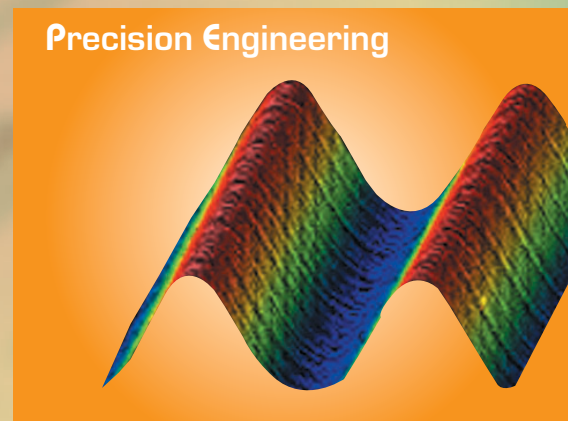
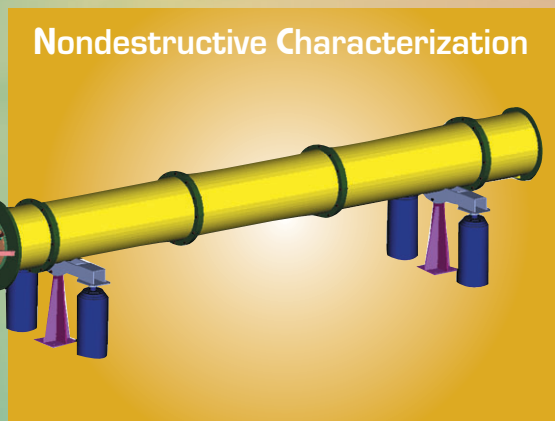
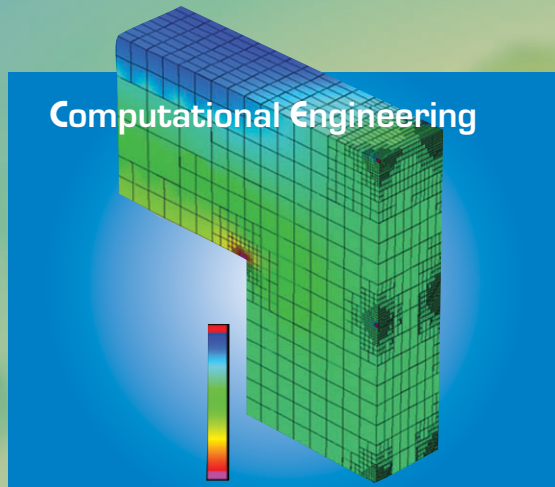
FY03 is our final year of this project. We have been working with various national agencies to continue our work for real applications. We have also published several papers for peer-reviewed publications and conferences.

In summary, we have developed UWB radios meeting the radio specifications we had hoped to achieve. Our final design has resulted in small-size, low-power, low-cost hand-held transceivers that can be networked for various national intelligence and defense applications. 



UWB communication transceiver.

Author Index



Author Index

Algazi, V. R.	21	Lehmann, J.	33
Aufderheide, M. B.	24	Madsen, N. K.	6
Azevedo, S. G.	21, 33	Mariella, Jr., R. P.	13
Barbee, T. W.	22, 24	Martz, H. E.	22, 24
Barty, A.	24	McCallen, D. B.	35
Becker, R. C.	8	Montesanti, R. C.	29
Behymer, E. M.	18	Morse, J. D.	15
Benett, W. J.	14	Myers, S. C.	34
Bennett, C. V.	18	Nederbragt, W. W.	22, 24
Benzel, D. M.	36	Nelson, K. E.	34
Bond, S. W.	18	Ness, K. D.	14
Bond, T. C.	17	Pannu, S. S.	16
Carlisle, K.	13	Pao, H.-Y.	9
Castillo, V. M.	7	Parsons, D.	3
Chambers, D. H.	21, 23	Pivovarov, M.	24
Champagne, N. J.	6	Puso, M. A.	5
Chang, J. T.	21	Quarry, M. J.	25
Chapman, H. N.	24	Reinhardt, C. E.	18
Chaung, F. Y. S.	16	Richards, J. B.	14
Chen, A. A.	14	Rodgers, A. J.	35
Christian, A. T.	14	Romero, C. E.	21
Clague, D. S.	4	Rose, J.	25
Dauffy, L. S.	33	Rose, K. A.	16
Dougherty, G. M.	16	Rubenchik, A. M.	13
Dowla, F. U.	36	Sale, K. E.	33
Du, Y.	18	Schneberk, D. J.	24
Felker, F. F.	7	Shirk, M. D.	13
Fisher, K. A.	25	Solberg, J. M.	3, 5
Gilmer, G. H.	13	Sopchak, D. A.	15
Haugen, P. C.	21	Sperry, V. R.	18
Han, I. Y.	18	Spiridon, A.	36
Harben, P. E.	34	Stone, G. F.	24
Harris, D. B.	34	Stratton, P. L.	14
Hartmann-Siantar, C. L.	33	Tkalcic, H.	35
Havstad, M. A.	16	Trebes, J. E.	34
Henderer, B. D.	33	Trumper, D. L.	29
Kallman, J. S.	17	Upadhye, R. S.	15
Khanaka, G. H.	17	Vargas, C.	22
Klingmann, J. L.	22, 29	Wagoner, J. L.	34
Kobayashi, N. P.	18	Weisgraber, T. H.	4, 14
Koch, J. A.	24	Welty, R. J.	18
Kozioziemski, B. J.	24	Wheeler, E. K.	14
Larsen, S. C.	34	White, D. A.	6
Leach, R. R.	21	Yoo, S. J.	18
Lehman, S. K.	23	Zumstein, J. M.	21

Manuscript Date April 2004
Distribution Category UC-42

This report has been reproduced directly from the best available copy.

Available for a processing fee to U.S. Department of Energy and its contractors in paper from
U.S. Department of Energy
Office of Scientific and Technical Information
P.O. Box 62
Oak Ridge, TN 37831-0062
Telephone: (865) 576-8401
Facsimile: (865) 576-5728
E-mail: reports@adonis.osti.gov

Available for sale to the public from
U.S. Department of Commerce
National Technical Information Service
5285 Port Royal Road
Springfield, VA 22161
Telephone: (800) 553-6847
Facsimile: (703) 605-6900
E-mail: orders@ntis.fedworld.gov
Online ordering: <http://www.ntis.gov/products/>

Or

Lawrence Livermore National Laboratory
Technical Information Department's Digital Library
<http://www.llnl.gov/library/>

This document was prepared as an account of work sponsored by an agency of the United States Government. Neither the United States Government nor the University of California nor any of their employees, makes any warranty, express or implied, or assumes any legal liability or responsibility for the accuracy, completeness, or usefulness of any information, apparatus, product, or process disclosed, or represents that its use would not infringe privately owned rights. Reference herein to any specific commercial products, process, or service by trade name, trademark, manufacturer, or otherwise, does not necessarily constitute or imply its endorsement, recommendation, or favoring by the United States Government or the University of California. The views and opinions of authors expressed herein do not necessarily state or reflect those of the United States Government or the University of California, and shall not be used for advertising or product endorsement purposes.

This work was performed under the auspices of the U.S. Department of Energy by the University of California, Lawrence Livermore National Laboratory under Contract W-7405-Eng-48.
ENG-03-0095-AD



Lawrence Livermore National Laboratory
University of California
P.O. Box 808, L-151
Livermore, California 94551



http://www_eng.llnl.gov/